JCTC Journal of Chemical Theory and Computation

Article

pubs.acs.org/JCTC

Flexible Boundaries for Multiresolution Solvation: An Algorithm for Spatial Multiscaling in Molecular Dynamics Simulations

Oliwia M. Szklarczyk,[†] Noah S. Bieler, Philippe H. Hünenberger, and Wilfred F. van Gunsteren*

Laboratory of Physical Chemistry, Department of Chemistry and Applied Biosciences, Swiss Federal Institute of Technology ETH, 8093 Zürich, Switzerland

Supporting Information

ABSTRACT: An algorithm is proposed for performing molecular dynamics (MD) simulations of a biomolecular solute represented at atomistic resolution surrounded by a surface layer of atomistic fine-grained (FG) solvent molecules within a bulk represented by coarse-grained (CG) solvent beads. The method, called flexible boundaries for multiresolution solvation (FBMS), is based on: (i) a three-region layering of the solvent around the solute, involving an FG layer surrounded by a mixed FG−CG buffer layer, itself surrounded by a bulk CG region; (ii) a definition of the layer boundary that relies on an effective distance to the solute surface and is thus adapted to the shape of the solute as well as adjusts to its conformational changes. The effective surface distance is defined by inverse-*n*th power averaging over the distances to all non-hydrogen solute atoms, and the layering is enforced by means of half-harmonic distance restraints, attractive for the FG molecules and repulsive for the CG beads. A restraint-free region at intermediate distances enables the formation of the buffer layer, where the FG and CG solvents can mix freely. The algorithm is tested and validated using the GROMOS force field and the associated FG (SPC) and CG (polarizable CGW) water models. The test systems include pure-water systems, where one FG molecule plays the role of a solute, and a deca-alanine peptide with two widely different solute shapes considered, α-helical and fully extended. In particular, as the peptide unfolds, the number of FG molecules required to fill its close-range solvation layer increases, with the additional molecules being provided by the buffer layer. Further validation involves simulations of four proteins in multiresolution FG/CG mixtures. The resulting structural, energetic, and solvation properties are found to be similar to those observed in corresponding pure FG simulations.

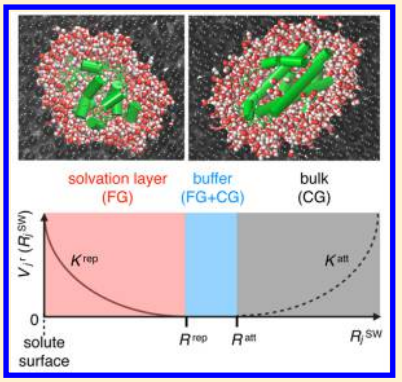

1. INTRODUCTION

Theoretical computational modeling to study biomolecular systems relies on the availability of powerful computers, along with efficient algorithms to exploit this computational power. In addition, the size of the simulated system and the time period covered by a simulation depend on the resolution of the molecular model used to represent this system: the finer the resolution, the smaller the system and the shorter the simulation period. For this reason, supra-atomic and supra-molecular coarse-grained (CG) models[1−8] have been proposed whose resolution is reduced compared to that of atomic level fine-grained (FG) models in order to increase the accessible system sizes and simulation lengths. Coarse-graining involves a reduction of the number of degrees of freedom. The selection of the degrees of freedom to be eliminated and those to be retained for studying the properties or processes of interest is one of the challenges when coarse-graining.[9−11] The interactions governing the eliminated vs retained degrees of freedom must be decoupled, leading to an effective interaction model that encompasses the average influence of the removed degrees of freedom on the remaining ones.[5,9,11,12] Generally, removing certain degrees of freedom will restrict the domain of application and transferability of a model. For example, a CG model for water may reproduce well the properties of the pure liquid under ambient conditions but fail to perform satisfactorily at other state points of the phase diagram.[13,14] In practice, the use of CG models makes sense only when the gain in speed brought by the use of a supra-atomic or supra-molecular level of resolution outweighs the loss in accuracy associated with the resolution decrease.

Molecular dynamics (MD) simulations using a CG representation for specific atom groups in a molecular system date back to the first studies of biomolecules. The united-atom representation,[15] in which the aliphatic CH, CH_2, and CH_3 groups as well as the CH_4 molecule are represented by a single Lennard-Jones particle, is a CG representation with respect to the atomic level. Yet, it is still generally considered to be an FG description with respect to supra-atomic or supra-molecular CG models that lump more than one non-hydrogen atoms into a bead. Many CG models of molecules in the condensed phase,[16−27] polymers,[1,28] or biomolecules[3,29−38] have been proposed and employed over the past decades.[2,4,5,7,39,40]

In order to avoid removing important degrees of freedom and interactions when coarse-graining, approaches that combine multiple levels of resolution, i.e., multiple grain levels or spatial

Received: May 1, 2015
Published: September 2, 2015

DOI: 10.1021/acs.jctc.5b00406
J. Chem. Theory Comput. 2015, 11, 5447−5463

scales, have been developed. For example, the quantum-mechanical/molecular-mechanical (QM/MM) scheme[41,42] combines nuclei-electron and atomic levels of resolution for different regions in the system, keeping the grain level of the particles fixed throughout the simulation. There are two main approaches applied in multiresolution MD simulations:[5]

(1) Multiscaling in time:
   (a) trajectories from CG simulations are mapped back to the FG level of resolution during postprocessing,[43−49] or
   (b) the system smoothly switches between the FG and CG representations over the course of a simulation, e.g., within a Hamiltonian replica-exchange scheme.[50−52]
(2) Multiscaling in space:
   (a) adaptive-resolution fixed-boundary schemes, where the resolution of a given particle changes in time depending on its position in space, e.g., as a function of the distance to a solute molecule, whereas the boundaries between regions of different resolution are fixed throughout the simulation,[53−59] or
   (b) flexible-boundary fixed-resolution schemes, where the boundaries between regions of different resolution change in time, e.g., adapting to the instantaneous shape of a solute molecule, whereas the resolution of the individual particles is fixed throughout the simulation.[60−63]

When using a supra-molecular CG solvent model to directly solvate an atomistic FG solute, the solute properties are often significantly distorted[64−70] due to an inaccurate representation of essential short-range interactions, such as hydrogen bonding, or a lack of solvation-shell structuring. This can be remedied either by developing specific force fields for hybrid simulations of FG solutes in CG solvents[71] or by inserting a number of FG solvent molecules around the solute.[5,11,60,72] The challenging aspects in the latter type of approach involving an FG solute embedded in an FG solvent layer, itself surrounded by a CG solvent bulk region, are: (i) to maintain the layering structure throughout the simulation, i.e., to prevent diffusion of the CG beads into the FG layer and of the FG molecules into the CG bulk region; (ii) to maintain a sufficient thickness of the FG layer throughout the simulation, irrespective of possibly occurring conformational changes in the solute, leading to corresponding changes in its shape and solvent-exposed surface area.

The simplest situation, although not the most physically realistic, is encountered when the FG and CG models spontaneously demix and the FG model presents a higher affinity for the surface of the FG solute. This is the case, for example, for mixtures of the fine-grained SPC water model[73] and the coarse-grained WT4 water model[19] because the corresponding self-solvation free enthalpies (SPC in SPC and WT4 in WT4) are more negative[63] than the cross-solvation ones (SPC in WT4 and WT4 in SPC). In this case, layering will occur and be maintained spontaneously around an FG solute immersed in an FG/CG solvent mixture, leading directly to a flexible-boundary fixed-resolution scheme.[63] However, spontaneous demixing is probably not a desirable property because if a CG bead is viewed as an effective cluster of multiple FG molecules, then FG molecules and CG beads should freely mix in all proportions. Most CG models are developed with the goal of achieving self- and cross-solvation free enthalpies of comparable magnitudes.[70,74] In this case, any method for simulating an FG solute in an FG/CG solvent mixture must include an algorithmic component that explicitly enforces the separation of the two solvents.

As an example, in ref 55, this separation is implemented within an adaptive-resolution fixed-boundary scheme. The particles move freely from one region of resolution to another via a hybrid region, in which the FG and CG interactions are smoothly transformed into one another by means of a continuous switching parameter. However, it is not possible to write a Hamiltonian for the system,[53,54] and an external thermodynamic force must be applied[75,76] to remedy density artifacts at the boundary between the regions of differing resolutions. An extension of the method formulated in terms of a global Hamiltonian has been recently proposed.[77]

Another example[62] of how the separation can be implemented employs a flexible-boundary fixed-resolution scheme. Here, the FG solute molecule carries special interaction sites termed virtual sites.[61] These act as virtual CG particles, with which the CG solvent beads interact through the standard MARTINI Lennard-Jones potential energy function.[3] The force due to the CG solvent on the virtual sites of the solute is distributed over all atoms of this molecule in a mass-weighted manner. However, the virtual-site approach alone is not sufficient to keep the two solvents separated, and the reported simulations[61] do not reproduce very accurately the properties of small test biomolecules compared to those observed in fully FG simulations. This is remedied in ref 62 by including an attractive restraining force from the solute virtual sites to the FG solvent molecules such that the FG layer adapts to the solute conformation.

A conceptually simpler and practically effective alternative to the above virtual-site scheme is proposed and tested in ref 60. There, half-harmonic attractive distance restraints are used to keep the FG molecules close to the center of mass (COM) of the solute. A comparable approach has also been formulated in ref 59 in terms of an adaptive-resolution fixed-boundary scheme relying on spherical boundaries. In both cases, the method enforces a spherical shape for the FG solvent layer around the solute, via restraints in ref 60 or via fixed spherical boundaries in ref 59. These methods work well provided that the tertiary structure of the solute molecule is relatively spherical and remains so throughout the simulation. In practice, however, solutes are seldom spherical, and a large number of FG solvent molecules must be used to cover the entire surface of the solute irrespective of its shape and possible variations thereof. This increases the computational cost which, in turn, may offset the gain achieved by coarse-graining part of the solvent.

In the present article, we introduce a method for multiscaling in space, in which the resolution of the particles is fixed throughout the simulation but the boundaries between the regions of different resolutions are flexible. This method will be referred to as flexible boundaries for multiresolution solvation (FBMS). The essential components of the proposed approach are (Figures 1 and 2): (i) a three-region layering of the solvent around the FG solute, involving an FG solvent layer for accurate short-range solvation, surrounded by a mixed FG−CG solvent buffer layer serving as a transition region and reservoir of particles of the two types, itself surrounded by a bulk CG solvent region to ensure a computationally inexpensive long-range solvation; (ii) a definition of the layer boundaries that relies on an effective distance to the solute surface, thus requiring a minimal number of FG molecules for a solute of nonspherical shape, and adapting to possible changes in this shape throughout the simulation.

DOI: 10.1021/acs.jctc.5b00406
J. Chem. Theory Comput. 2015, 11, 5447−5463

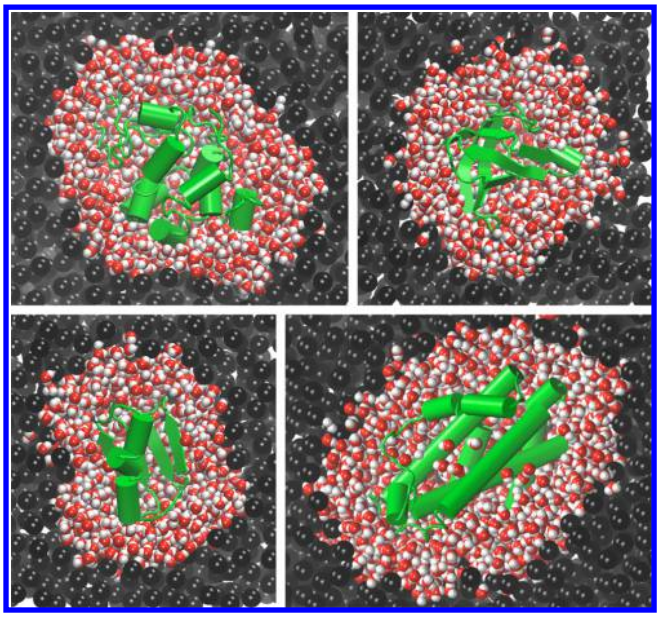

Figure 1. Principle underlying the flexible boundaries for multi-resolution solvation (FBMS) method. Fine-grained (FG) solvent molecules, here atomistic water (red and white spheres denote oxygen and hydrogen atoms, respectively), and coarse-grained (CG) water beads (black spheres denote CW particles) rearrange around the solute molecule (a protein with secondary structure shown in green) such that the FG solvent forms a layer around the solute surface and the CG solvent forms the bulk region. Illustrative trajectory configurations are shown for four proteins, from left to right and top to bottom: hen egg-white lysozyme (HEWL), major cold shock protein (CspA), G-protein (GP), and chorismate mutase (CM).

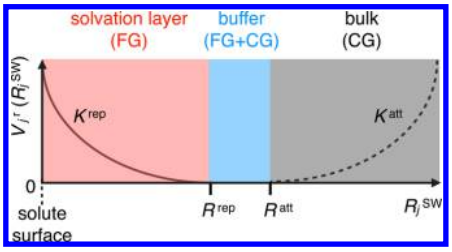

Figure 2. Form of the terms $V_j^r(R_j^{SW})$ in the restraining potential energy function of eq 3. The term corresponding to a solvent molecule (FG) or bead (CG) j depends on the corresponding surface-weighted distance R_j^{SW} of eq 1, the latter representing an effective distance to the solute surface. A half-harmonic attractive restraint (eq 4) with a force constant K^{att} prevents the FG molecules from diffusing far beyond the reference distance R^{att}. A half-harmonic repulsive restraint (eq 5) with a force constant K^{rep} prevents the CG beads from approaching far below the reference distance R^{rep}. The choice $R^{rep} < R^{att}$ ensures the formation of a buffer region (eq 2) where the FG and CG solvents can mix in free proportions.

If a solute undergoes a large conformational transition, e.g. folding or unfolding of a polypeptide, then the shape and volume of its close-range solvation shell will change, and so will the number of FG solvent molecules required to fill this shell. The CG solvent beads should be prevented from entering this volume, as their direct interaction with the solute may distort its properties. In the FBMS approach, both requirements are fulfilled by introducing a buffer region that contains a varying proportion of FG to CG solvents. This buffer serves in particular as a reservoir of FG solvent molecules for the close-range solvation layer when the solute unfolds or as an absorber when the solute folds. It is introduced by applying concurrently half-harmonic attractive distance restraints between solute atoms and the FG solvent molecules along with half-harmonic repulsive distance restraints between solute atoms and the CG solvent beads. The associated reference distances, i.e., the distances at which the two types of restraints are switched on or off, are selected so that the corresponding regions of zero restraint energy overlap over a certain range of distances, which defines the buffer region (Figure 2). The attractive distance restraints to the FG solvent molecules are applied only to a single atom of the molecule, e.g., the oxygen atom for water. The same applies to the CG beads if more than one bead is used to represent the molecules of a given solvent or if the model involves auxiliary, e.g., polarization,[78] sites. In both cases, the single selected site is referred to in the following as the reference site of the FG molecule or CG bead.

If the layer boundaries are to be defined in terms of the distance to the solute surface, then the above restraints could be applied using the distance between a particular FG solvent molecule or CG solvent bead and the closest solute atom. However, the identity of this closest solute atom will frequently change, leading to forces on the solute atoms that are switched on and off in time, i.e., are discontinuous. Furthermore, the most exposed solute atoms will always be the ones exclusively affected by the restraints, which may in turn significantly alter their dynamic properties. For this reason, in the FBMS approach, the restraints are made to be dependent on an effective surface distance R^{SW}, referred to as the surface-weighted distance. This distance is a continuous function of the coordinates of all solute atoms but effectively depends on the coordinates of the few atoms closest to a particular FG solvent molecule or CG solvent bead. The use of this effective distance is inspired from nuclear magnetic resonance (NMR) Overhauser enhancement (NOE) assignment and structure refinement methods,[79,80] and it has also been used in docking approaches based on ambiguous distance restraints derived from experimental data.[81,82] It is defined as

$$R_j^{SW} = R^{SW}(\mathbf{r}^{N_{su}}, \mathbf{r}_j) = \left(\sum_{i=1}^{N_{su}} r_{ij}^{-n}\right)^{-1/n} \quad (1)$$

where N_{su} is the number of non-hydrogen solute atoms, $\mathbf{r}^{N_{su}} = (\mathbf{r}_1,\mathbf{r}_2,...,\mathbf{r}_{N_{su}})$, $\mathbf{r}_i$ denotes the Cartesian position vector of non-hydrogen solute atom i, $\mathbf{r}_j$ is the Cartesian position vector of the reference site of a FG solvent molecule or CG solvent bead j, and $r_{ij} = |\mathbf{r}_i - \mathbf{r}_j|$. The notation R_j^{SW} stands for the surface-weighted distance of a particular solvent site j, where the implicit dependence on $\mathbf{r}^{N_{su}}$ is omitted for simplicity. The exponent n in eq 1 is an arbitrary number larger than 1. In practice, n is taken to be an integer with $n \gg 1$. The metric R^{SW} is known in mathematics as a p-norm,[83] where $p = -n$, but the associated metric spaces (L^p-spaces) are almost exclusively studied in the context of positive exponents, typically, $p \geq 1$. The dependence of the surface-weighted distance R_j^{SW} on the individual solute−solvent distances r_{ij} in eq 1 ensures that, for sufficiently large n, only solute atoms i that are close to the solvent molecule or bead j will contribute to the restraining force on j. The restraining therefore acts in terms of the distance to the solute surface, ensuring flexible layer boundaries that remain adapted to its shape at any time.

In the remainder of this article, we define the FBMS approach in detail, describe its implementation, and investigate the effect of its defining parameters on the simulation results. All simulations presented in this work use the GROMOS 54A7 force field[84] for

DOI: 10.1021/acs.jctc.5b00406
J. Chem. Theory Comput. 2015, 11, 5447−5463

the FG solute along with the SPC model[73] for FG water and the supra-molecular polarizable CGW model[78] for CG water. For testing purposes, we investigate four types of systems in order of increasing complexity. First, a box filled with FG water molecules is considered, in which one reference molecule is tagged as solute. Second, a box containing a mixture of FG water molecules and CG water beads is considered, in which one reference FG molecule is again tagged as solute. Third, the FBMS algorithm is applied to an alanine deca-peptide, considering both a folded, α-helical, and an unfolded, fully extended, solute conformation. Here, the solute consists of $N_{su} > 1$ non-hydrogen atoms, and the surface-weighted distance R^{SW} now depends on the value of the exponent n. The ability of the method to keep the peptide solvated by a layer of FG molecules upon unfolding is investigated. Finally, we consider four different proteins solvated in an FG/CG water mixture with FBMS restraints applied. For various combinations of the parameters, the simulated structural, energetic, and solvation properties of the proteins are compared to those observed in purely FG simulations.[60] The investigation of the four types of test systems results in a set of recommended parameters for use in multiscale MD simulations of biomolecules under FBMS restraints.

2. METHODS

2.1. Restraining Algorithm. In the FBMS method, the solvent molecules surrounding a solute biomolecule should ideally consist of a pure FG layer, then a buffer region where mixing between FG molecules and CG beads is allowed, and finally a region of pure CG bulk solvent (Figures 1 and 2), with the layer boundaries being adjusted to the instantaneous shape of the solute. This is enforced through the use of appropriate restraining forces depending on two reference distances, R^{att} and R^{rep}, with $R^{rep} < R^{att}$, and on the surface-weighted distance of eq 1. Here, R^{att} defines the furthest possible surface-weighted distance to which an FG molecule can diffuse without being subject to attractive restraints, and R^{rep}, the shortest possible surface-weighted distance at which a CG solvent bead can approach the solute without being subject to repulsive restraints. The thickness Δr_B of the buffer region is defined as the difference between R^{att} and R^{rep}, i.e.

$$\Delta r_B = R^{att} - R^{rep} \tag{2}$$

The restraining potential energy V^r is defined as

$$V^r(\mathbf{r}^{N_{su}}, \mathbf{r}^{N_{sv}}) = \sum_{j=1}^{N_{sv}} V_j^r(R_j^{SW})$$

$$\text{with } V_j^r(R_j^{SW}) = \begin{cases} V^{att}(R_j^{SW}) & \text{if } j \in \text{FG} \\ V^{rep}(R_j^{SW}) & \text{if } j \in \text{CG} \end{cases} \tag{3}$$

where N_{sv} is the number of solvent FG or CG reference sites, $\mathbf{r}^{N_{sv}} = (\mathbf{r}_1,\mathbf{r}_2,...,\mathbf{r}_{N_{sv}})$, and $R_j^{SW} = R^{SW}(\mathbf{r}^{N_{su}},\mathbf{r}_j)$ is the surface-weighted distance of eq 1 for solvent reference site j, which depends on the positions of the N_{su} non-hydrogen atoms of the solute. For an FG solvent site j, V_j^r is a half-harmonic attractive restraining potential energy function V^{att} given by

$$V^{att}(R_j^{SW}) = \begin{cases} 0 & \text{for } R_j^{SW} < R^{att} \\ \frac{1}{2}K^{att}(R_j^{SW} - R^{att})^2 & \text{for } R_j^{SW} \geq R^{att} \end{cases} \tag{4}$$

For a CG solvent site j, V_j^r is a half-harmonic repulsive restraining potential energy function V^{rep} given by

$$V^{rep}(R_j^{SW}) = \begin{cases} \frac{1}{2}K^{rep}(R_j^{SW} - R^{rep})^2 & \text{for } R_j^{SW} \leq R^{rep} \\ 0 & \text{for } R_j^{SW} > R^{rep} \end{cases} \tag{5}$$

The forces acting on the atoms can be obtained using the chain rule based on the derivatives of the potential energy V^r (eq 3) with respect to R_j^{SW}, along with the derivatives of the surface-weighted distance R_j^{SW} (eq 1) with respect to $\mathbf{r}_i$ and $\mathbf{r}_j$. The attractive restraining force acting on an FG solvent site j is then

$$\mathbf{f}_j^{att} = \begin{cases} 0 & \text{for } R_j^{SW} < R^{att} \\ K^{att}(R_j^{SW} - R^{att})(R_j^{SW})^{n+1} \sum_{i=1}^{N_{su}} (r_{ij}^{-n-2}\mathbf{r}_{ij}) & \text{for } R_j^{SW} \geq R^{att} \end{cases} \tag{6}$$

where $\mathbf{r}_{ij} = \mathbf{r}_i - \mathbf{r}_j$ and the repulsive restraining force acting on a CG solvent site j is

$$\mathbf{f}_j^{rep} = \begin{cases} k^{rep}(R_j^{SW} - R^{rep})(R_j^{SW})^{n+1} \sum_{i=1}^{N_{su}} (r_{ij}^{-n-2}\mathbf{r}_{ij}) & \text{for } R_j^{SW} \leq R^{rep} \\ 0 & \text{for } R_j^{SW} > R^{rep} \end{cases} \tag{7}$$

Accordingly, the total restraining force acting on a non-hydrogen solute atom i from all the restrained solvent molecules is

$$\mathbf{f}_i^r = -\sum_{j=1}^{N_{sv}} [K^X(R_j^{SW} - R^X)(R_j^{SW})^{n+1} r_{ij}^{-n-2}\mathbf{r}_{ij}] \tag{8}$$

where X is either att or rep, depending on the grain nature of the solvent site j.

When using distance restraints between the solute and the solvent molecules or beads, the restraining forces may provide a non-negligible contribution to the virial of the system. In constant-pressure simulations, neglecting this contribution can lead to an inappropriate box volume at equilibrium which, in extreme cases, may cause numerical errors and an explosion of the system. The contribution of the FBMS restraints to the virial was included in all simulations reported in this work.

2.2. Analysis of the Simulations. Structural, energetic, and solvation properties of the biomolecular systems investigated, such as the radial distribution functions $g(r)$, atom-positional root-mean-square deviations (RMSD) relative to the crystallographic structure, atom-positional root-mean-square fluctuations (RMSF), radii of gyration R_{gyr}, hydrogen-bond numbers and occurrences, and secondary-structure contents (DSSP) were calculated as described in ref 66 using the GROMOS++ analysis programs.[85]

2.2.1. Surface-Weighted Distance R^{SW} and Splitting Entropy Measure $M(R^{SW})$. For a solute containing more than one non-hydrogen atom, the surface-weighted distance R_j^{SW} between the solute and a solvent site j will not be equal to the distance r_j^{min} from the closest solute atom, since each non-hydrogen solute atom i contributes to the R_j^{SW} distance. One may quantify the contribution of each solute−solvent distance r_{ij} to the surface-weighted distance R_j^{SW} of solvent site j by means of the coefficients

DOI: 10.1021/acs.jctc.5b00406
J. Chem. Theory Comput. 2015, 11, 5447−5463

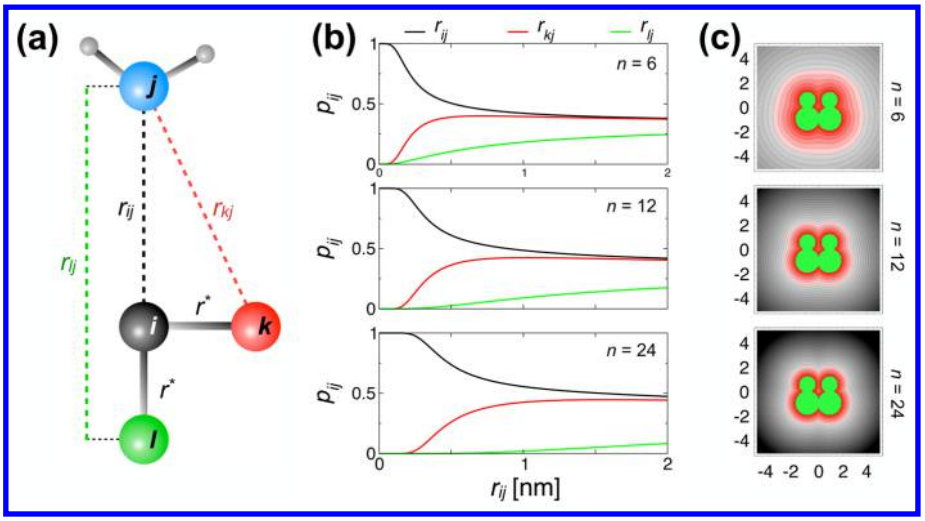

Figure 3. Toy system to illustrate the properties of the surface-weighted distance R^{SW} depending on the exponent n in eq 1. (a) Three surface atoms, i, k, and l, of a toy solute molecule are placed in the corners of a right triangle with the length of the catheti equal to $r^* = 0.15$ nm. A water molecule with oxygen atom j is placed at a certain distance from the surface of the solute. (b) Dependence of the coefficient p_{ij} of eq 9 to the surface-weighted distance R^{SW} on the exponent n for the three solute atoms, i, k, and l, and for solvent molecule j, shown as a function of the distance r_{ij} to the closest solute atom i. The colors of the curves correspond to the colors of the solute atoms in panel (a). (c) Contours of R^{SW}, in units of nanometers, in the plane of a cross-section of an asymmetrically shaped solute molecule (central green shape) consisting of 3613 atoms. For low exponents (top graph), the shape of the solute molecule is lost at short R^{SW} and the layers around the solute become spherical near the solute, whereas for higher exponents (middle and bottom graphs), the shape of the solute is distinguishable at larger R^{SW} distances and the layers preserve the shape of the solute.

$$p_{ij} = \left(\frac{r_{ij}}{R_j^{SW}}\right)^{-n} \text{ with } \sum_{i=1}^{N_{su}} p_{ij} = 1 \quad \forall\, j \tag{9}$$

The quantity p_{ij} is not the contribution of r_{ij} to R_j^{SW} but that of r_{ij}^{-n} to $(R_j^{SW})^{-n}$.

Ideally, only a small number of solute atoms, primarily the solvent-exposed ones, should contribute significantly to the surface-weighted distance R_j^{SW}, i.e., exhibit non-negligible p_{ij} coefficients. Whether this holds and within what distance range strongly depends on the exponent n in eq 1, as illustrated in Figure 3. In this figure, we consider a toy system consisting of a triatomic solute and a single solvent molecule. The three solute atoms labeled i, k, and l are placed at the corners of a right triangle, and the bond lengths r_{ik} and r_{il} are both set to 0.15 nm (Figure 3a). In the limit of infinite distances from the solute, each solute atom contributes equally to R_j^{SW} (Figure 3b). However, at finite distances, the solute atom closest to the solvent molecule j, i.e., atom i in Figure 3a, has the largest contribution, and the one most remote, i.e., atom l in the figure, has the smallest contribution. The relative weighting depends on the value of the exponent n, as illustrated in Figure 3b. The green curve which corresponds to the contribution of atom l, is the lowest curve in all graphs. For $n = 6$ at a distance $r_{ij} = 1$ nm, the contribution of this atom is less than 20% (top panel). For $n = 12$, this contribution decreases to less than 10% (middle panel), and for $n = 24$ to less than 3% (bottom panel). Similarly, as shown by the red curve, the contribution of atom k, the other solute surface atom, to R_j^{SW} at $r_{ij} = 0.3$ nm decreases from 30% for $n = 6$ to less than 10% for $n = 24$. With a larger exponent n, the surface-weighted distance R_j^{SW} remains a close approximation to r_j^{min} over a longer range of distances, and the contours of R^{SW} match the shape of a solute at increasingly large distances from this solute before becoming essentially spherical (Figure 3c).

A splitting entropy measure[86] M_j can be used to assess the distribution of the p_{ij} coefficients

$$M_j = 1 + \frac{1}{\ln N_{su}} \sum_{i=1}^{N_{su}} p_{ij} \ln p_{ij} \tag{10}$$

In the limiting case $r_j^{min} \to \infty$, corresponding to a solvent site j at a very large distance from the solute surface, all of the individual r_{ij} distances become nearly equal, and one has $p_{ij} = N_{su}^{-1}$ for all solute atoms i, so $M_j = 0$. In the limiting case $r_j^{min} \to 0$, corresponding to a solvent site j at the solute surface, a single solute atom i contributes to the surface-weighted distance, and one has $p_{ij} = 1$ for this specific solute atom and $p_{ij} = 0$ for all the others, so $M_j = 1$. In these limiting cases, one may thus write

$$\begin{aligned} &r^{min} \to \infty: \quad R^{SW} \to (N_{su})^{-1/n} r^{min} \quad \text{and} \quad M \to 1 \\ &r^{min} \to 0: \quad R^{SW} \to r^{min} \quad \text{and} \quad M \to 0 \end{aligned} \tag{11}$$

where the index j has been omitted to underline that these are, in fact, general properties of the R^{SW} metric for a given solute configuration $\mathbf{r}^{N_{su}}$. In practice, R^{SW} lies between these two extremes and is always smaller than r^{min}. The exponent n effectively controls the range up to which R^{SW} remains close to r^{min} upon increasing the distance from the solute (Figure 3c). For small n, R^{SW} will be smaller than r^{min} already at a close range due to significant contributions from the buried solute atoms. Thus, in the case of FG molecules, it may happen that attractive restraints are not applied even though $r_j^{min} > R^{att}$. Similarly, in the case of CG beads, it may happen that repulsive restraints are applied even though $r_j^{min} > R^{rep}$. These peculiarities can be alleviated by choosing a sufficiently high exponent n. Yet, n should not be made too large to ensure that the restraining forces remain distributed over multiple solute surface atoms.

The splitting entropy measure M_j of eq 10 can be resolved as a function of R_j^{SW} by averaging over all solvent sites j and over time, leading to a function that is denoted $M(R^{SW})$. This function represents a useful indicator to assess the extent of similarity between R^{SW} and r^{min} as well as the extent of spreading of the

DOI: 10.1021/acs.jctc.5b00406
J. Chem. Theory Comput. 2015, 11, 5447−5463

Table 1. Simulation Parameters and Simulated Properties for the Test Systems Involving FG Water Molecules within Bulk FG Water[a]

system	R^{att} [nm]	R^{rep} [nm]	$K^{att} = K^{rep}$ [kJ mol^{-1} nm^{-2}]	V_{box} [nm^3]	ρ [kg m^{-3}]	V_{nonb}^{FG-FG} [kJ mol^{-1}]	D [10^{-3}nm^2 ps^{-1}]
FG	∞	0		30.7	974.5	−41.6	4.3
FG	0.8	0.5	60	30.7	975.8	−41.6	3.6
FG	0.8	0.5	300	30.7	975.3	−41.6	3.6

[a]The systems consist of 1000 FG water molecules. One reference molecule plays the role of a solute, 24 molecules are subjected to attractive FBMS restraints, and 975 molecules are subjected to repulsive FBMS restraints. The restraints are applied with respect to the OW atom of the reference molecule. Different combinations of the restraining parameters R^{att}, R^{rep}, K^{att}, and K^{rep} are considered. The time-averaged properties reported based on 10 ns simulations are the box volume V_{box}, the density ρ, the total potential energy (Lennard-Jones plus electrostatic) per molecule V_{nonb}^{FG-FG}, and the self-diffusion coefficient D. See Figure 4 for the corresponding radial distribution functions.

Table 2. Simulation Parameters and Simulated Properties for the Test Systems Involving FG Water Molecules within Bulk CG Water[a]

system	R^{att} [nm]	R^{rep} [nm]	K^{att} [kJ mol^{-1} nm^{-2}]	K^{rep} [kJ mol^{-1} nm^{-2}]	V_{box} [nm^3]	V_{att} [kJ mol^{-1}]	V_{rep} [kJ mol^{-1}]	V_{nonb}^{FG-FG} [kJ mol^{-1}]
FG/CG	∞	0			245.0			−0.03
FG/CG	1.2	0.8	60	300	247.9	0.39	0.02	0.00
FG/CG	0.8	2.0	60	300	280.8	1.04	0.03	0.00
FG/CG	∞	2.0		300	313.9		0.01	0.00

[a]The systems consist of 58 FG water molecules and 1618 CG water beads. One reference FG molecule plays the role of a solute, the 57 other FG molecules are subjected to attractive FBMS restraints, and the 1618 CG beads are subjected to repulsive FBMS restraints. The restraints are applied with respect to the OW atom of the reference FG molecule. Different combinations of the restraining parameters R^{att}, R^{rep}, K^{att}, and K^{rep} are considered. The time-averaged properties reported based on 10 ns simulations are the box volume V_{box}, the restraint energy V^{att} per FG solvent molecule, the restraint energy V^{rep} per CG solvent bead, and the total potential energy $V_{nonb}^{su\text{-}CG}$ (Lennard-Jones plus electrostatic) between the solute molecule and the CG solvent beads per single CG bead. See Figure 5 for other simulated properties.

restraint forces over the solute surface for different choices of the FBMS parameters.

2.2.2. Local Volumetric Fractions ν_{FG} and ν_{CG}. The local distribution of the two solvent types around the solute molecule was analyzed in terms of local volumetric fractions ν_s. More precisely, given a volume element in the system, the local volumetric fractions ν_{FG} and ν_{CG} of solvents of types FG and CG, respectively, are given by

$$\nu_{FG} = \frac{V_{FG} n_{FG}}{V_{FG} n_{FG} + V_{CG} n_{CG}} \text{ and } \nu_{CG} = 1 - \nu_{FG} \tag{12}$$

where n_{FG} and n_{CG} are the average numbers of molecules of the two types found in the volume element based on the positions of the corresponding reference sites, and V_{FG} and V_{CG} denote the corresponding single-particle volumes. The ratio of these volumes was approximated as $V_{CG}/V_{FG} \approx 5$, where FG and CG correspond to the atomistic SPC model[73] and the coarse-grained CGW model, respectively.[78] The volumetric fractions ν_{FG} and ν_{CG} of eq 12 were resolved as a function of either R_j^{SW} or r_j^{min} by binning and averaging over all solvent sites j and over time, leading to functions denoted $\nu_s(R^{SW})$ and $\nu_s(r^{min})$, respectively, where the s subscript stands for FG or CG.

2.3. Test Systems. *2.3.1. FG Water Molecules within Bulk FG Water.* As a first test system, a cubic box of approximate edge length 3.1 nm containing 1000 FG water molecules was simulated. One reference molecule played the role of a solute, with attractive restraints applied to 24 other molecules and repulsive restraints applied to the remaining 975 molecules. This permitted to study the effect of different values for the FBMS parameters (Table 1) in a very simple context.

2.3.2. FG Water Molecules within Bulk CG Water. As a second test system, a cubic box of approximate edge length 6.3 nm containing a mixture of 58 FG and 1618 CG molecules was simulated. Again, one reference FG molecule played the role of a solute, with attractive restraints applied to the 57 other FG molecules, corresponding to an FG layer of initial thickness Δr_L^0 equal to 0.8 nm, and with repulsive restraints applied to the 1618 CG beads. This situation corresponds to FBMS restraints applied relative to a single non-hydrogen solute atom, the oxygen atom of the reference FG water molecule. Therefore, the surface-weighted distance R_j^{SW} is here exactly equal to the real distance between the solute atom and a solvent particle j. This simple setup permitted to test the influence of the restraining parameters, namely, the reference restraining distances and force constants (Table 2), on the distributions of the two solvent types around the reference FG water molecule.

2.3.3. Helical and Extended Conformations of Deca-alanine in FG/CG Water. As a third test system, an alanine deca-peptide was considered. The peptide was capped with an acetyl group at its N-terminus and an *N*-methylamide group at its C-terminus. Starting from a canonical α-helical conformation, it was solvated in a layer of FG water molecules of initial thickness Δr_L^0 equal to 0.4, 0.6, or 0.8 nm. The thickness Δr_L^0 is defined here in terms of the surface-weighted distance R^{SW} from the solute so that the corresponding numbers N_{FG} of FG molecules (Table 3) varied between the different systems depending on the exponent n. The peptide and FG layer were further solvated by CG beads to fill a cubic computational box with an initial edge length of 5.9 nm. Since the initial box size was the same for all systems, the number N_{CG} of CG water beads also varied between the systems (Table 3). Starting from this setup in an α-helical conformation, the peptide was progressively unfolded into a fully extended conformation. Simulations with FBMS restraints were performed for both the α-helical and extended conformations, in both cases maintaining the structure by applying dihedral angle restraints on the backbone ϕ and ψ dihedral angles. The

DOI: 10.1021/acs.jctc.5b00406
J. Chem. Theory Comput. 2015, 11, 5447−5463

Table 3. Simulation Parameters for the Test Systems Involving a Deca-alanine Peptide in FG/CG Water Mixtures with FBMS Restraints[a]

		n = 6		n = 12		n = 18	
system	Δr_L^0 [nm]	N_{FG}	N_{CG}	N_{FG}	N_{CG}	N_{FG}	N_{CG}
FG/CG	0.4	79	1396	49	1405		
FG/CG	0.6	297	1278	160	1303	145	1306
FG/CG	0.8	654	1197	327	1271	275	1279
FG		6972	0				

[a]The parameters reported are the numbers N_{FG} of FG solvent molecules and N_{CG} of CG solvent beads in the different systems. For comparison, the number N_{FG} in a pure FG system (N_{CG} = 0) with the same box size is also given (last line). For the FG/CG systems, these numbers are determined by the selected exponent n, the initial peptide conformation (here, α-helical), the initial FG layer thickness Δr_L^0, and the initial volume of the computational box (here, cube of edge 5.9 nm). See Tables 4 and 5 as well as Figures 6−8 for other simulation parameters and simulated properties.

attractive and repulsive restraining force constants were set to (K^{att}, K^{rep}) = (300, 600) kJ mol^{-1} nm^{-2}. The corresponding reference distances R^{att} and R^{rep} were varied (Tables 4 and 5), and three values of the exponent n (6, 12, or 18) were considered. For comparison purposes, additional simulations were also performed involving the peptide in an FG/CG mixture without FBMS restraints, i.e., with reference distances set to $R^{att} = \infty$ and $R^{rep} = 0$.

The choice of deca-alanine in water as a test system was motivated by the goal of having a simple peptide that can be easily brought into a helical or an extended conformation. This was achieved by varying only the backbone torsional angles, i.e., without introducing the complexity of flexible side chains and Coulomb forces between charged side chains. The deca-alanine peptide was used to demonstrate how the FBMS algorithm can accommodate the change in the number of molecules required to fill the FG layer when a solute undergoes a large conformational transition.

2.3.4. Proteins in FG/CG Water. Finally, four proteins were simulated in multiresolution FG/CG water mixtures. Here, the FBMS method was tested with respect to its influence on the structural, energetic, and solvation properties of the biomolecules as compared to previously performed simulations in pure FG water[66] or in FG/CG water mixtures with restraints applied to the COM of the protein. The four proteins considered are (Figure 1) hen egg-white lysozyme (HEWL, PDB:[87] 1AKI), major cold shock protein (CspA, PDB:[88] 1MJC), G-protein (GP, PDB:[89] 1PGB), and chorismate mutase (CM, PDB:[90] 2FP2). The setup of the simulations involved an initial FG layer thickness Δr_L^0 of either 0.6 or 0.8 nm. The corresponding numbers of FG water molecules and CG water beads are listed in Table 6. For each system, three values of the exponent n (12, 18 or 24) were considered. The restraining force constants (K^{att}, K^{rep}) were set to (300, 600) kJ mol^{-1} nm^{-2} as in the simulations of the deca-alanine peptide. The reference restraining distances (R^{att}, R^{rep}) were set to (0.8, 0.7) nm or (1.0, 0.9) nm for Δr_L^0 = 0.6 and 0.8 nm, respectively.

2.4. Simulation Protocols. All simulations described in this article were performed using the parameters of the GROMOS 54A7 force field[84] and with the aid of the GROMOS11 software package.[91,92] The FG water molecules were represented by the atomistic simple-point-charge (SPC) water model,[73] with the

Table 4. Simulation Parameters and Simulated Properties for the Test Systems Involving a Deca-alanine Peptide in FG/CG Water Mixtures with FBMS Restraints[a]

R^{att} [nm]	R^{rep} [nm]	V_{box} [nm^3]		V^{att} [kJ mol^{-1}]		V^{rep} [kJ mol^{-1}]		$V_{nonb}^{su\text{-}CG}$ [kJ mol^{-1}]	
FG/CG, Δr_L^0 = 0.6 nm, α-helix									
		n = 12	n = 18	n = 12	n = 18	n = 12	n = 18	n = 12	n = 18
∞	0.0	203.8		0.0		0.0		−0.25	
0.6	0.4	201.5	201.7	0.34	0.35	0.00	0.00	−0.07	−0.07
0.6	0.5	201.3	201.5	0.33	0.34	0.01	0.01	−0.06	−0.07
0.8	0.5	200.9	201.2	0.27	0.26	0.00	0.00	−0.11	−0.11
0.8	0.6	201.0	201.2	0.21	0.22	0.03	0.03	−0.07	−0.08
0.8	0.7	201.3	201.4	0.16	0.16	0.02	0.02	−0.04	−0.05
1.0	0.7	201.9	201.9	0.19	0.20	0.03	0.03	−0.05	−0.06
1.0	0.8	203.5	203.0	0.19	0.17	0.04	0.03	−0.03	−0.04
FG/CG, Δr_L^0 = 0.6 nm, extended									
		n = 12	n = 18	n = 12	n = 18	n = 12	n = 18	n = 12	n = 18
∞	0.0	203.7		0.0		0.0		−0.37	
0.6	0.4	201.0	201.1	0.36	0.37	0.00	0.00	−0.13	−0.13
0.6	0.5	200.9	200.9	0.31	0.34	0.02	0.02	−0.11	−0.12
0.8	0.5	200.6	200.8	0.33	0.31	0.00	0.00	−0.19	−0.19
0.8	0.6	201.1	200.9	0.26	0.23	0.06	0.05	−0.10	−0.10
0.8	0.7	202.4	202.3	0.19	0.20	0.05	0.05	−0.05	−0.06
1.0	0.7	203.3	202.9	0.23	0.21	0.06	0.06	−0.06	−0.06
1.0	0.8	207.3	205.7	0.22	0.20	0.05	0.05	−0.03	−0.03

[a]The results correspond to simulations of the peptide in either an α-helical (top block) or a fully extended (bottom block) conformation for an initial FG layer thickness Δr_L^0 = 0.6 nm (initial refers to the α-helical conformation), with restraints applied using the exponents n = 12 or 18 along with different reference distances R^{att} and R^{rep}. In all cases, the restraining force constants (K^{att}, K^{rep}) were set to (300, 600) kJ mol^{-1} nm^{-2}. The time-averaged properties reported based on 5 ns simulations are the box volume V_{box}, the restraint energy V^{att} per FG solvent molecule, the restraint energy V^{rep} per CG solvent bead, and the total potential energy $V_{nonb}^{su\text{-}CG}$ (Lennard-Jones plus electrostatic) between the solute molecule and the CG solvent beads per CG bead. See Tables 3 and 5 as well as Figures 6−8 for other simulation parameters and simulated properties.

DOI: 10.1021/acs.jctc.5b00406
J. Chem. Theory Comput. 2015, 11, 5447−5463

Table 5. Simulation Parameters and Simulated Properties for the Test Systems Involving a Deca-alanine Peptide in FG/CG Water Mixtures with FBMS Restraints[a]

R^{att} [nm]	R^{rep} [nm]	V_{box} [nm^3]		V^{att} [kJ mol^{-1}]		V^{rep} [kJ mol^{-1}]		$V_{nonb}^{su\text{-}CG}$ [kJ mol^{-1}]	
		FG/CG, Δr_L^0 = 0.8 nm, α-helix							
		n = 12	n = 18	n = 12	n = 18	n = 12	n = 18	n = 12	n = 18
∞	0.0	205.6		0.0		0.0		−0.23	
0.8	0.4	201.2	200.9	0.20	0.21	0.00	0.00	−0.02	−0.04
0.8	0.6	201.1	201.0	0.19	0.18	0.00	0.00	−0.02	−0.03
0.8	0.7	201.3	200.9	0.18	0.17	0.00	0.00	−0.02	−0.02
1.0	0.7	200.6	200.5	0.14	0.12	0.01	0.01	−0.02	−0.03
1.0	0.8	200.7	200.4	0.12	0.12	0.02	0.01	−0.02	−0.02
1.0	0.9	201.0	200.5	0.10	0.10	0.03	0.03	−0.02	−0.02
1.2	0.7	200.3	200.4	0.15	0.13	0.01	0.01	−0.03	−0.03
1.2	0.8	200.4	200.3	0.12	0.12	0.02	0.02	−0.02	−0.03
1.2	1.0	204.3	203.8	0.11	0.11	0.05	0.04	−0.02	−0.02
		FG/CG, Δr_L^0 = 0.8 nm, extended							
		n = 12	n = 18	n = 12	n = 18	n = 12	n = 18	n = 12	n = 18
∞	0.0	205.1		0.0		0.0		−0.34	
0.8	0.4	200.5	200.5	0.21	0.22	0.00	0.00	−0.09	−0.10
0.8	0.6	200.5	200.4	0.17	0.16	0.01	0.02	−0.04	−0.05
0.8	0.7	200.7	200.5	0.14	0.12	0.02	0.02	−0.03	−0.04
1.0	0.7	200.6	200.4	0.12	0.13	0.02	0.03	−0.03	−0.04
1.0	0.8	201.0	200.9	0.12	0.12	0.05	0.05	−0.03	−0.03
1.0	0.9	201.2	201.0	0.09	0.10	0.05	0.05	−0.02	−0.02
1.2	0.7	200.5	200.6	0.15	0.16	0.04	0.04	−0.04	−0.05
1.2	0.8	201.1	201.9	0.09	0.12	0.05	0.05	−0.03	−0.03
1.2	1.0	210.9	206.5	0.13	0.12	0.05	0.04	−0.01	−0.01

[a]The results correspond to simulations of the peptide in either an α-helical (top block) or a fully extended (bottom block) conformation for an initial FG layer thickness Δr_L^0 = 0.8 nm (initial refers to the α-helical conformation), with restraints applied using the exponents n = 12 or 18 along with different reference distances R^{att} and R^{rep}. In all cases, the restraining force constants (K^{att}, K^{rep}) were set to (300, 600) kJ mol^{-1} nm^{-2}. The time-averaged properties reported based on 5 ns simulations are the box volume V_{box}, the restraint energy V^{att} per FG solvent molecule, the restraint energy V^{rep} per CG solvent bead, and the total potential energy $V_{nonb}^{su\text{-}CG}$ (Lennard-Jones plus electrostatic) between the solute molecule and the CG solvent beads per CG bead. See Tables 3 and 4 as well as Figures 6−8 for other simulation parameters and simulated properties.

Table 6. Simulation Parameters and Simulated Properties for the Test Systems Involving a Protein in FG/CG Water Mixtures with FBMS Restraints[a]

	n = 12					n = 18					n = 24				
protein	N_{FG}	N_{CG}	V^{att} [kJ mol^{-1}]	V^{rep} [kJ mol^{-1}]	$V_{nonb}^{su\text{-}CG}$ [kJ mol^{-1}]	N_{FG}	N_{CG}	V^{att} [kJ mol^{-1}]	V^{rep} [kJ mol^{-1}]	$V_{nonb}^{su\text{-}CG}$ [kJ mol^{-1}]	N_{FG}	N_{CG}	V^{att} [kJ mol^{-1}]	V^{rep} [kJ mol^{-1}]	$V_{nonb}^{su\text{-}CG}$ [kJ mol^{-1}]
	FG/CG, Δr_L^0 = 0.6 nm, R^{att} = 0.8 nm, R^{rep} = 0.7 nm														
HEWL	1159	2680	0.51	0.007	−0.03	1065	2696	0.67	0.008	−0.04	1044	2702	0.77	0.007	−0.05
CspA	784	1491	0.48	0.012	−0.15	718	1504	0.62	0.010	−0.17	704	1508	0.67	0.011	−0.17
GP	664	1386	0.42	0.011	−0.25	614	1393	0.56	0.009	−0.27	599	1396	0.60	0.010	−0.28
CM	1567	3871	0.46	0.006	−0.12	1442	3885	0.61	0.006	−0.14	1401	3893	0.67	0.006	−0.14
	FG/CG, Δr_L^0 = 0.8 nm, R^{att} = 1.0 nm, R^{rep} = 0.9 nm														
HEWL	1864	2538	0.35	0.008	0.00	1698	2572	0.52	0.008	−0.01	1640	2587	0.58	0.008	−0.01
CspA	1316	1385	0.36	0.013	−0.11	1176	1412	0.47	0.014	−0.13	1143	1418	0.54	0.013	−0.13
GP	1124	1284	0.33	0.011	−0.13	1016	1315	0.40	0.001	−0.15	989	1324	0.47	0.010	−0.15
CM	2449	3673	0.32	0.006	−0.09	2225	3729	0.45	0.006	−0.10	2166	3740	0.54	0.006	−0.11

[a]The parameters reported are the numbers N_{FG} of FG solvent molecules and N_{CG} of CG solvent beads. The time-averaged properties reported based on 20 ns simulations are the restraint energy V^{att} per FG solvent molecule, the restraint energy V^{rep} per CG solvent bead, and the total potential energy $V_{nonb}^{su\text{-}CG}$ (Lennard-Jones plus electrostatic) between the solute molecule and the CG solvent beads per single CG bead. Two combinations of the initial FG layer thickness Δr_L^0 and of the reference distances R^{att} and R^{rep} are considered (top and bottom blocks), along with three values of the exponent n (groups of columns). The restraining force constants (K^{att}, K^{rep}) were set to (300, 600) kJ mol^{-1} nm^{-2} in all cases. See Figures 9−13 for other simulated properties.

oxygen atom (OW) as a reference site for the FBMS restraining. The CG water beads were represented by the polarizable CGW water model,[78] with the central site (CW) as a reference particle for the FBMS restraining. Their interaction with the SPC water molecules was modeled as described in refs 74 and 78. The SHAKE procedure[93] was employed to constrain the bond lengths and the hydrogen−hydrogen distances within the FG water molecules.

DOI: 10.1021/acs.jctc.5b00406
J. Chem. Theory Comput. 2015, 11, 5447−5463

Newton's equations of motion were integrated using the leapfrog scheme[94] with a time step of 2 fs. Periodic boundary conditions were applied based on cubic computational boxes. All simulations were performed at constant temperature and pressure. The average temperature was kept at 298 K by weak coupling[95] to heat baths with a coupling time of 0.1 ps. The average pressure was kept at 1 atm by weak coupling[95] to a pressure bath using isotropic scaling and a group-based virial, with a coupling time of 0.5 ps and an isothermal compressibility of $4.575 \cdot 10^{-4}$ kJ^{-1} mol nm^3, as appropriate for biomolecular systems.[96]

The configurations and energies during the MD production runs, 10 ns for the pure water boxes, 5 ns for the helical and extended conformations of deca-alanine, and 20 ns for each of the four proteins, were saved every 1 ps (water boxes) or 2 ps (deca-alanine and four proteins) for analysis.

2.4.1. Purely FG Simulations. The pure FG water box was subjected to a 100 ps equilibration followed by 10 ns production. The deca-alanine peptide was energy minimized in vacuum starting from a canonical α-helix conformation, solvated in SPC water, and progressively thermalized for a total time of 120 ps. It was simulated for 5 ns in the α-helical conformation, enforced by harmonic dihedral-angle restraints[97] on the ϕ and ψ backbone dihedral angles with reference values set to $(-60°, -50°)$. The reference values were then gradually decreased over four steps of 100 ps. Thereafter, the peptide was again simulated for 5 ns in the extended conformation, as enforced by ϕ and ψ dihedral-angle restraints with the reference values set to $(-180°, -180°)$. The dihedral-angle restraints relied on a force constant of 100 kJ mol^{-1} rad^{-2} in all cases. The simulation protocol for the purely FG simulations of the four proteins is described in ref 66. The simulations of the pure FG water box involved a single heat bath, whereas the purely FG simulations involving a biomolecular solute involved separate coupling of the solute and solvent to two different heat baths.

In all purely FG simulations, a triple-range cutoff scheme[98] with short- and long-range cutoff radii set to 0.8 and 1.4 nm, respectively, was employed to treat the van der Waals and electrostatic interactions. The interactions within the short-range cutoff radius were calculated every time step, whereas the interactions in the intermediate range were calculated every 5 steps and assumed constant in between. The mean effect of the electrostatic interactions beyond the long-range cutoff radius was represented by a reaction-field force[99,100] with a relative dielectric permittivity set to 66, as appropriate for the SPC water model.[101]

2.4.2. Multiresolution FG/CG Simulations. Starting from the final configurations obtained in the corresponding purely FG simulations, all of the systems considered were modified such that an FG water layer of a specified initial thickness Δr_L^0 was kept around the solute molecule and the rest of the box was filled with CG water beads. These configurations were used as initial structures for the multiresolution simulations with FBMS restraints. For each parameter combination tested, a separate minimization and equilibration of the initial configuration was performed. The CG solvent was energy minimized while positionally restraining the solute atoms and FG solvent molecules using a force constant of $2.5 \cdot 10^4$ kJ mol^{-1} nm^{-2}. Initial velocities were then assigned from a Maxwell–Boltzmann distribution at 60 K, and the system was subjected to a 100 ps thermalization at constant volume. Over this period, the position restraints on the solute atoms and FG solvent molecules were gradually weakened while increasing the temperature in five steps of about 60 K until it reached 298.15 K. While weakening the position restraints, the attractive and repulsive force constants of the FBMS restraints were gradually increased to their final values. In the case of the deca-alanine peptide, the dihedral angle restraints were applied throughout the equilibration process and the MD production simulation to preserve the initial α-helical or extended conformation. Finally, a 40 ps constant pressure simulation completed the equilibration, with no restraints other than the FBMS restraints. During equilibration and production, the solute and FG solvent were weakly coupled to a common heat bath, and the CG solvent to a separate heat bath.

The multiresolution FG/CG simulations were performed using a triple-range cutoff scheme[98] with short- and long-range cutoff radii set to 1.4 and 2.0 nm, respectively. A reaction-field approximation[99,100] was applied for the long-range electrostatic interactions with a relative dielectric permittivity set to 78.5, corresponding to the experimental value for water[102] as well as the value for the CGW water model.[78] The dielectric permittivity within the cutoff sphere[74] was set to 1.0, 2.5, or 2.3 for the FG–FG, CG–CG, and FG–CG interactions, respectively. The FBMS restraining forces were updated every time step.

3. RESULTS AND DISCUSSION

3.1. FG Water Molecules within Bulk FG Water. To test the influence of the parameters of the proposed method on the properties of a simple system consisting of solvent only, simulations were performed involving pure FG water boxes without and with FBMS restraints applied. When using the restraints, a reference water molecule was singled out to play the role of a solute, 24 other molecules were selected to play the role of the FG solvation layer, and the remaining 975 molecules were mimicking the bulk solvent. The volume occupied by a droplet of 25 FG molecules is about equal to that of a sphere of 0.56 nm radius. The attractive restraints were applied beyond a reference distance R^{att} = 0.8 nm, and the repulsive restraints up to a reference distance R^{rep} = 0.5 nm relative to the reference water molecule (Table 1). The results of these simulations are reported in Table 1 and Figure 4.

The box volume V_{box}, water density ρ, and average nonbonded interaction energy per molecule V_{nonb}^{FG-FG} are barely affected by the application of the restraints. The restraints slightly reduce the

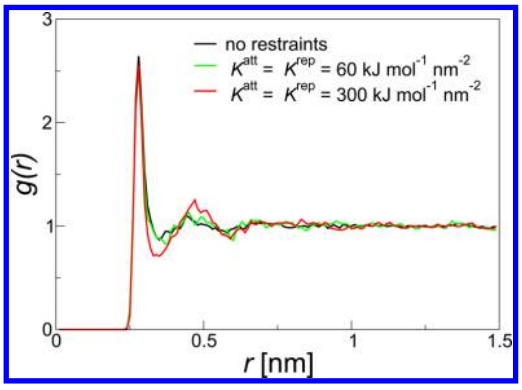

Figure 4. Oxygen–oxygen radial distribution functions $g(r)$ for the test systems involving FG water molecules within bulk FG water. One reference water molecule plays the role of the solute, and different combinations of the restraining parameters are tested; see Table 1. The radial distribution functions are based on 10 ns simulations and calculated considering only pairs involving the reference water molecule. The restraining reference distances (R^{att}, R^{rep}) in the FBMS simulations were set to (0.8, 0.5) nm.

DOI: 10.1021/acs.jctc.5b00406
J. Chem. Theory Comput. 2015, 11, 5447–5463

diffusion coefficient D from its normal value of $4.3{\cdot}10^{-3}$ nm^2 ps^{-1} for SPC water to $3.6{\cdot}10^{-3}$ nm^2 ps^{-1} in the presence of the restraints. This is expected as, in particular, the attractive restraints bind 25 molecules together in terms of diffusion properties. The oxygen−oxygen radial distribution functions $g(r)$ calculated only for pairs involving the reference water molecule playing the role of the solute show no changes upon introducing the restraints with $K^{att} = K^{rep} = 60$ kJ mol^{-1} nm^{-2}. A slightly enhanced structure is visible in the second hydration shell at 0.48 nm when the force constants are increased to 300 kJ mol^{-1} nm^{-2}. Most likely, this results from the onset of the repulsive restraints at $R^{rep} = 0.5$ nm, leading to small perturbations in the radial and orientational properties of the molecules around this distance.

3.2. FG Water Molecules within Bulk CG Water. The next test system consists of FG/CG water boxes with a reference FG water molecule playing the role of a solute along with different combinations of the restraining reference distances R^{att} and R^{rep} and force constants K^{att} and K^{rep}. The FG water layer in these systems comprises 57 FG molecules, which corresponds to an initial layer thickness Δr_L^0 of 0.8 nm. The results are shown in Figure 5 in terms of local volumetric fractions ν_s and illustrative system configurations for a chosen subset of parameter combinations (Table 2). Values for specific simulated properties can also be found in Table 2. The results including all parameter combinations as well as corresponding values for the average box volume V_{box} are provided as Supporting Information, Figures S1 and S2, respectively.

Applying only attractive restraints to the FG molecules ($R^{att} < \infty$, $R^{rep} = 0$) is not sufficient to keep the CG beads from coming close to the solute (Figure S1; also illustrated for the G-protein in Figure S3). When using only repulsive restraints to the CG beads ($R^{att} = \infty$, $R^{rep} > 0$), these no longer come close to the solute, but the FG molecules diffuse into the bulk (Figure S1, red curve in Figure 5, top, and Figure 5d). This leads to similar volumetric fractions in the bulk region as those observed over the entire system in the absence of FBMS restraints (compare with the black curve in Figure 5, top, and with Figure 5a). Moreover, in the absence of attractive restraints, the box volume increases when R^{rep} becomes larger than 0.4 nm (Figure S2). In summary, applying solely attractive or solely repulsive restraints to separate FG and CG solvents is not sufficient, and both types of restraints are required to achieve the desired layering around the solute.

When restraints are applied to both FG and CG solvents ($R^{att} < \infty$, $R^{rep} > 0$), the box volume does not deviate compared to the simulation without restraints, provided that R^{att} and R^{rep} do not exceed 1.2 and 0.8 nm, respectively (Figure S2). The average restraint energies per molecule or bead in the simulation with $R^{att} = 1.2$ nm, $R^{rep} = 0.8$ nm, $K^{att} = 60$ kJ mol^{-1} nm^{-2}, and $K^{rep} = 300$ kJ mol^{-1} nm^{-2} (Figure 5b) are 0.4 and 0.02 kJ mol^{-1} for the FG and CG solvents, respectively, and the solute does not interact with the CG solvent (blue curve in Figure 5, top, and second row in Table 2). Thus, the distance R^{rep} should not be made larger than the initial thickness Δr_L^0 of the FG solvation layer.

Whether FG molecules tend to solvate in CG water or CG beads to solvate in FG water depends on the relative solvation free enthalpies of FG molecules and CG beads in FG water or CG water. Based on ref 74, at 298 K and 1 atm, the solvation free enthalpies of an SPC molecule in SPC water, of an SPC molecule in CGW water, of a CGW bead in SPC water, and of a CGW bead in CGW water are −29.3, −26.2, −10.5, and −16.4 kJ mol^{-1}, respectively. These values represent infinite-dilution limits, but they strongly suggest that the solvation of both SPC molecules and CGW beads in a SPC/CGW mixture of arbitrary

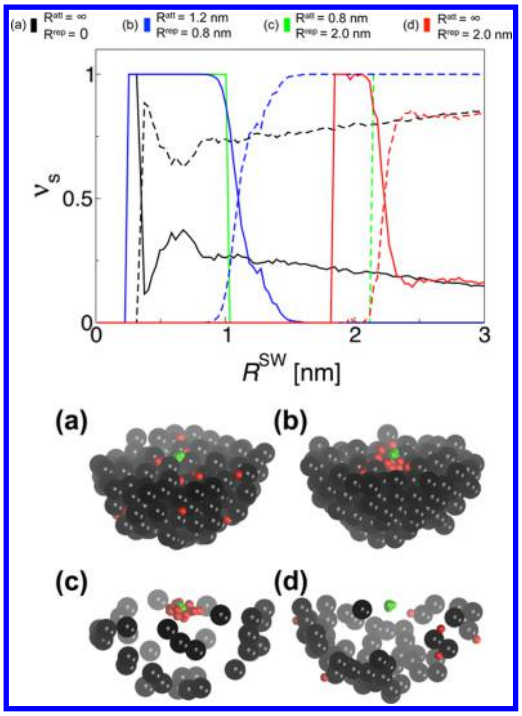

Figure 5. Simulated properties and illustrative configurations for the test systems involving FG water molecules within bulk CG water. The systems consist of one reference FG molecule playing the role of the solute (molecule shown in green), 57 other FG molecules (oxygen atoms shown in red), and 1618 CG water beads (shown in black). Different combinations of restraining parameters are tested; see Table 2. The top graph shows local volumetric fractions ν_s calculated using eq 12 and averaged over 10 ns simulation time and over the FG molecules (ν_{FG}, solid lines) or CG beads (ν_{CG}, dashed lines), and displayed as $\nu_s(R^{SW})$, where R^{SW} corresponds to the surface-weighted distance between solute and solvent (eq 1). The illustrative configurations (a−d) represent cross-sections through the (x,y) plane of the computational box within a 2.4 nm radius around the reference water molecule. Shown are last configurations from the simulations with (R^{att}, R^{rep}) equal to (∞, 0) nm (a), (1.2, 0.8) nm (b), (0.8, 1.2) nm (c), and (∞, 2.0) nm (d), corresponding to the curves of different colors in the top graph. See also Figures S1 and S2 in the Supporting Information for additional parameter combinations and the influence of the restraining on the box volume, respectively.

composition is always a spontaneous process associated with a sizable decrease in free enthalpy. Given such a physically realistic situation in terms of mixing properties, it is expected that relatively high values of the force constants K^{att} and K^{rep} are required to enforce the segregation of the two types of water into separate layers. Too high values should be avoided, however, because of the risk of introducing boundary artifacts. Based on Figures S1 and S2, optimal values for the two force constants considering the SPC and CGW models are on the order of 50−500 kJ mol^{-1} nm^{-2} for K^{att} and 500−1000 kJ mol^{-1} nm^{-2} for K^{rep}. For other models with weaker, physically less realistic, mixing properties, or even a spontaneous tendency to demix,[63] appropriate separation might be achieved using much lower force constants or even no restraints at all.

3.3. Helical and Extended Conformations of Deca-alanine in FG/CG Water. In the case of the atomistic alanine deca-peptide, a solute consisting of more than one non-hydrogen atom i, the surface-weighted distance R_j^{SW} of the solute to a solvent site j depends on multiple r_{ij} distances. In this case, the exponent n in eq 1 becomes of importance (Figure 3) because it

DOI: 10.1021/acs.jctc.5b00406
J. Chem. Theory Comput. 2015, 11, 5447−5463

affects the restraining forces in eqs 6−8. Based on the results obtained from the simulations of the mixed FG/CG water boxes, a number of reasonable parameter combinations for the FBMS algorithm were selected and tested for the two different conformations, α-helical or extended, of the peptide in mixed FG/CG water. The results are reported in Tables 4 and 5 as well as Figures 6−8. More details can also be found in Supporting Information Figures S4 and S5.

With an FG layer of initial thickness Δr_L^0 = 0.4 nm, initial referring to the layer around the α-helical conformation, the number of FG molecules is insufficient to fill the first solvation shell of the peptide irrespective of n, especially in the extended conformation (Figure 6 top). The CG solvent beads come too close to the solute, with average values of the nonbonded interaction energy $V_{nonb}^{su\text{-}CG}$ between the solute and the CG beads reaching −0.5 kJ mol^{-1} per bead (data not shown). For an FG solvation layer of initial thickness Δr_L^0 = 0.6 nm (Figure 6, middle), the first solvation shell of the peptide is appropriately filled by FG molecules in both conformations and $V_{nonb}^{su\text{-}CG}$ is reduced to about −0.1 kJ mol^{-1} in the presence of restraints (Table 4), to be compared with values of about −0.3 kJ mol^{-1} when the restraints are switched off. The box volume V_{box} is not significantly affected by the restraints, except for the simulation with (R^{att}, R^{rep}) = (1.0, 0.8) nm, in which it increases substantially upon unfolding the peptide. The lowest average restraining energies V^{att} per FG solvent molecule for both α-helical and extended conformations are observed in the simulation with (R^{att}, R^{rep}) = (0.8, 0.7) nm. For larger (R^{att}, R^{rep}) values, the restraining energies V^{att} per FG molecule and V^{rep} per CG bead slightly increase, but the interaction energy $V_{nonb}^{su\text{-}CG}$ between the CG beads and the peptide is reduced (see also Figure S4). Similar observations and trends also hold in the simulations with an FG layer of initial thickness Δr_L^0 = 0.8 nm (Figure 6, bottom, Table 5, and Figure S5).

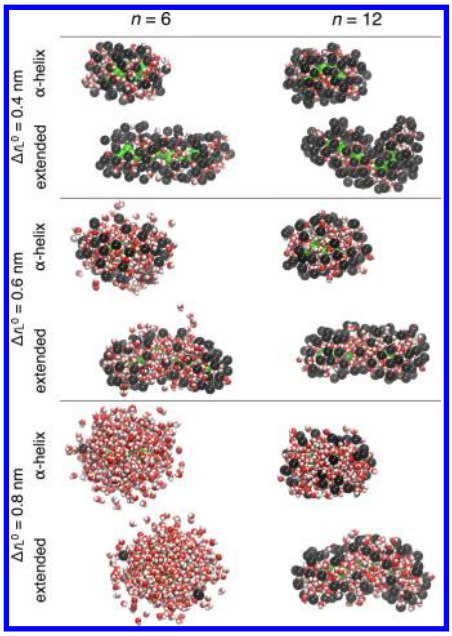

Figure 6. Illustrative configurations for the test systems involving a deca-alanine peptide in FG/CG water mixtures with FBMS restraints. The configurations are taken from pairs of 5 ns simulations of the peptide in either an α-helical or a fully extended conformation for three different initial thicknesses Δr_L^0 of the FG layer. The left and right columns correspond to two different exponents n in eq 1. Shown are all of the FG water molecules present in the system along with the CG solvent beads within 1 nm from the surface of the peptide. The color coding is the same as that in Figure 1. In all cases, (K^{att}, K^{rep}) = (300, 600) kJ mol^{-1} nm^{-2}, R^{att} = Δr_L^0 + 0.2 nm, and R^{rep} = Δr_L^0 + 0.1 nm.

The exponent n has a significant influence on the local volumetric fractions v_s of FG and CG solvents around the peptide calculated using eq 12. This influence is illustrated in Figure 7.

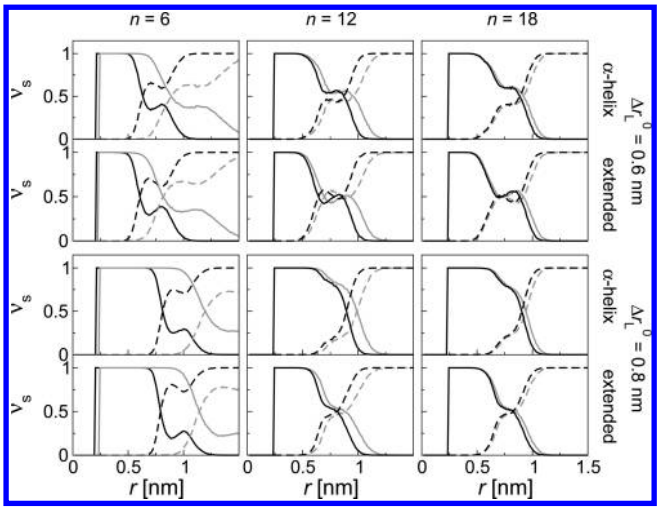

Figure 7. Local volumetric fractions v_s for the test systems involving a deca-alanine peptide in FG/CG water mixtures with FBMS restraints. The fractions are calculated using eq 12 based on pairs of 5 ns simulations of the peptide in either an α-helical or a fully extended conformation for two different initial thicknesses Δr_L^0 of the FG layer. The left, middle, and right columns correspond to three different exponents n in eq 1. The local volumetric fractions v_s are averaged over all FG molecules (v_{FG}, solid lines) or CG beads (v_{CG}, dashed lines) and displayed as $v_s(R^{SW})$ or $v_s(r^{min})$, where R^{SW} and r^{min} correspond to the surface-weighted distance between solute and solvent (black curves) or to the minimum distance between solute and solvent (gray curves), respectively. In all cases, (K^{att}, K^{rep}) = (300, 600) kJ mol^{-1} nm^{-2}, R^{att} = Δr_L^0 + 0.2 nm, and R^{rep} = Δr_L^0 + 0.1 nm. See also Figures S4 and S5 in the Supporting Information for additional parameter combinations.

The surface-weighted distance R^{SW} is always smaller than the distance r^{min} to the closest solute atom i (eq 11), and the exponent n controls how close the value of R^{SW} is to the value of r^{min}.

For n = 6 (Figure 7, left column), the distances R^{SW} are much lower than r^{min}, which results in differences between the local volumetric fractions $v_s(R^{SW})$ (black curves) and $v_s(r^{min})$ (gray curves). This effect is already noticeable at 0.4 nm from the surface of the solute when Δr_L^0 = 0.6 nm (0.7 nm when Δr_L^0 = 0.8 nm). The FBMS restraining scheme is defined in terms of R^{SW}, and the $v_s(R^{SW})$ curves present the expected features, e.g., a mixing of the two solvents in a buffer layer of thickness Δr_B between R^{rep} and R^{att}. However, the minimal distance r^{min} is a better measure of the actual distance to the solute surface and, for n = 6, the corresponding curves $v_s(r^{min})$ are smeared toward larger distances. In practice, this means that the true thicknesses of the FG and buffer layers, as measured in terms of r^{min}, are larger than would be anticipated from the values of Δr_L^0 and Δr_B, respectively. This is also reflected in the twice larger number of FG molecules required to set up the system with n = 6 compared to the corresponding systems with n = 12 or 18 for a given choice of Δr_L^0 (Table 3).

Upon increasing the exponent n to 12 or 18, the local volumetric fractions $v_s(R^{SW})$ and $v_s(r^{min})$ agree increasingly well

DOI: 10.1021/acs.jctc.5b00406
J. Chem. Theory Comput. 2015, 11, 5447−5463

with each other (Figure 7, middle and right columns). Here also, the expected three-layer structure is clearly achieved, with a pure FG layer, a mixed buffer layer, and a pure CG bulk region. However, for these larger exponents, the parameters Δr_B and Δr_L^0 become essentially equivalent to layer thicknesses in terms of surface distances. This is not only convenient for the setup of the simulated system, where the values selected for these parameters have a more intuitive interpretation, but also because it ensures that the FG and buffer layers follow more closely the shape of the solute surface.

The splitting entropy measure M of eq 10 reflects how close the surface-weighted distance R^{SW} is to the actual closest distance r^{min} to the solute (eq 11). As a particle moves away from the surface of the solute into the bulk, M evolves from 1 (value at contact) to 0 (value at infinite distance), and R^{SW}, from 0 (approximately as r^{min} at short distances) to ∞ (approximately as $N_{su}^{-1/n} r^{min}$ at large distances). The $M(R^{SW})$ curves from simulations with the three values of the exponent and different initial layer thicknesses are shown in Figure 8.

For $n = 6$, the $M(R^{SW})$ curves decrease abruptly from 1 at $R^{SW} = 0$ to values close to zero. This indicates that the switch from R^{SW} representing a distance to the surface to R^{SW} representing an average distance to the solute (weighted by $N_{su}^{-1/n}$) is very rapid. This observation reflects the poor overlap between the local volumetric fractions $v_s(R^{SW})$ and $v_s(r^{min})$ for $n = 6$.

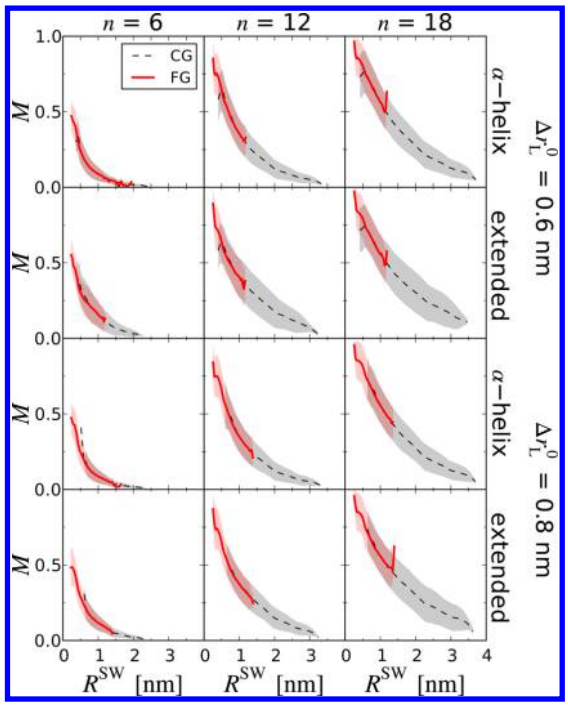

Figure 8. Splitting entropy measures M for the test systems involving a deca-alanine peptide in FG/CG water mixtures with FBMS restraints. The results are calculated using eq 10 based on pairs of 5 ns simulations of the peptide in either an α-helical or a fully extended conformation for two different initial thicknesses Δr_L^0 of the FG layer. The left, middle, and right columns correspond to three different exponents n in eq 1. The splitting entropy measure is averaged over all FG molecules (solid red lines) or over all CG beads (dashed black lines) and displayed as $M(R^{SW})$, where R^{SW} corresponds to the surface-weighted distance between solute and solvent, and the bin width was set to 0.06 nm. The shaded areas around the curves indicate the standard deviation around the mean. In all cases, $(K^{att}, K^{rep}) = (300, 600)$ kJ mol^{-1} nm^{-2}, $R^{att} = \Delta r_L^0 + 0.2$ nm, and $R^{rep} = \Delta r_L^0 + 0.1$ nm.

Upon increasing the exponent to $n = 12$ or 18, the $M(R^{SW})$ curves become far less steep. As a result, R^{SW} matches much better a surface distance over the relevant range, resulting in a closer agreement between $v_s(R^{SW})$ and $v_s(r^{min})$. For this reason, the FG layer also adjusts better to the shape of the solute at short range. Still, for both values of the exponent, $M(R^{SW})$ remains well below 1 for any distance where restraints can be active ($R^{SW} \geq R^{rep}$), ensuring that the restraint forces are distributed over the solute surface atoms.

The exponents $n = 12$ or 18 both appear to be good choices. The values of $V_{nonb}^{su\text{-}CG}$ are not significantly different between the corresponding simulations (Tables 4 and 5). The exponent $n = 18$ leads to a layering that follows slightly more closely the features of the solute surface, whereas $n = 12$ leads to a somewhat more extensive spreading of the restraint forces over the solute surface atoms. The selection of the reference restraining distances as $R^{att} = \Delta r_L^0 + 0.2$ nm and $R^{rep} = \Delta r_L^0 + 0.1$ nm also seems to be appropriate. Therefore, these represent the recommended choices for the application of the FBMS method to biomolecules.

3.4. Proteins in FG/CG Water. To test whether the main structural, energetic, and solvation properties of biomolecules are preserved when using multiresolution FG/CG solvation with FBMS restraints, four proteins were considered, namely, hen egg white lysozyme (HEWL), cold shock protein A (CspA), G-protein (GP), and chorismate mutase (CM) (see Figure 1). Two different values of the initial FG layer thickness Δr_L^0 and three values of the exponent n were tested (Table 6). The results are reported in Table 6 and Figures 9−13. More details can be found in Supporting Information Figures S6−S14.

In Figure 9, the RMSD values from the corresponding crystal structures[87−90] are compared to those observed in the fully FG simulations reported in ref 60. Note that in the latter simulations the nonbonded cutoff radii were set to 0.8 and 1.4 nm, whereas in the present FG/CG simulations, these values are set to 1.4 and 2.0 nm. Thus, an entirely similar behavior of the proteins should not be expected. In the case of HEWL, CspA, and GP, the RMSD values agree well with those observed in the purely FG simulations. For CM, the purely FG simulation shows substantial deviations from the crystal structure, which is no longer the case in the FG/CG simulations. Yet, the radius of gyration calculated for the backbone atoms agrees well for all four proteins (Figure S6). The large RMSD for CM is mainly due to a large displacement of the C-terminus affecting residues 158−163 (Figure S7). This effect occurs in both the purely FG and mixed FG/CG simulations. However, the C-terminus moves farther away from the crystal structure in the purely FG system.

In Figures 10 and 11, a similar comparison between fully FG simulations and the present FG/CG simulations is performed in terms of the RMSF values for the backbone C_α atoms and for the last non-hydrogen atoms of the side chains, respectively. The results are again found to agree well for the four proteins. In the case of HEWL, the FG/CG simulations with $\Delta r_L^0 = 0.6$ nm evidence differences of up to 0.1 nm, mainly in the unstructured regions of the protein. At the C-terminus, the differences reach 0.3 nm for the backbone, but no significant differences are observed for the side chains. In the FG/CG solvent simulations of CspA, the backbone and side-chain RMSF values deviate from the fully FG ones by nearly 0.2 nm in the unstructured region between residues 57 and 64. The GP protein also has some slight deviations of up to 0.1 nm, again in the unstructured regions comprising turns. In CM, the largest differences of up to 0.2 nm occur in the simulation with $\Delta r_L^0 = 0.6$ nm and $n = 12$, in the

DOI: 10.1021/acs.jctc.5b00406
J. Chem. Theory Comput. 2015, 11, 5447−5463

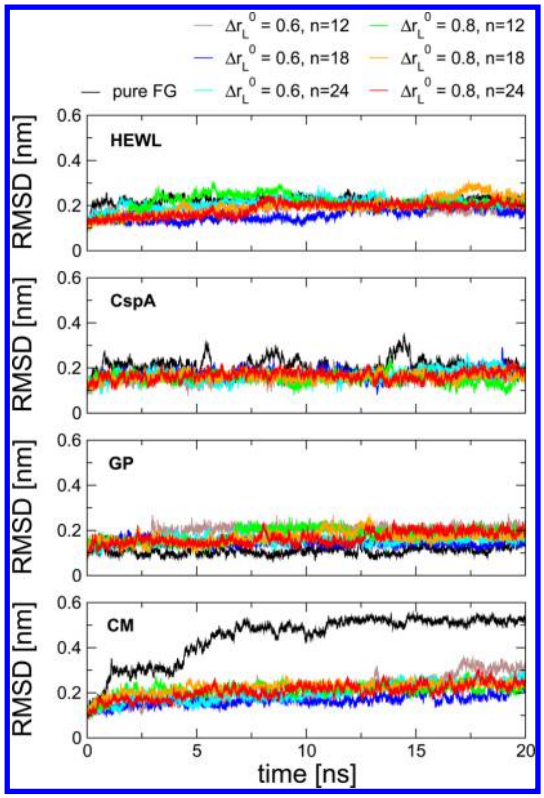

Figure 9. Atom-positional root-mean-square deviations (RMSD) of the backbone carbon, nitrogen, and oxygen atoms with respect to the crystal structures of the HEWL, CspA, GP, and CM proteins. Simulations of the four proteins in pure FG solvent (black) are compared to FG/CG systems with FBMS restraints involving an FG water layer of initial thickness Δr_L^0 = 0.6 nm and an exponent n = 12 (brown), Δr_L^0 = 0.6 nm and n = 18 (blue), Δr_L^0 = 0.6 nm and n = 24 (light blue), Δr_L^0 = 0.8 nm and n = 12 (green), Δr_L^0 = 0.8 nm and n = 18 (orange), or Δr_L^0 = 0.8 nm and n = 24 (red), surrounded by bulk CG water. See Table 6 for the parameters corresponding to the different simulations.

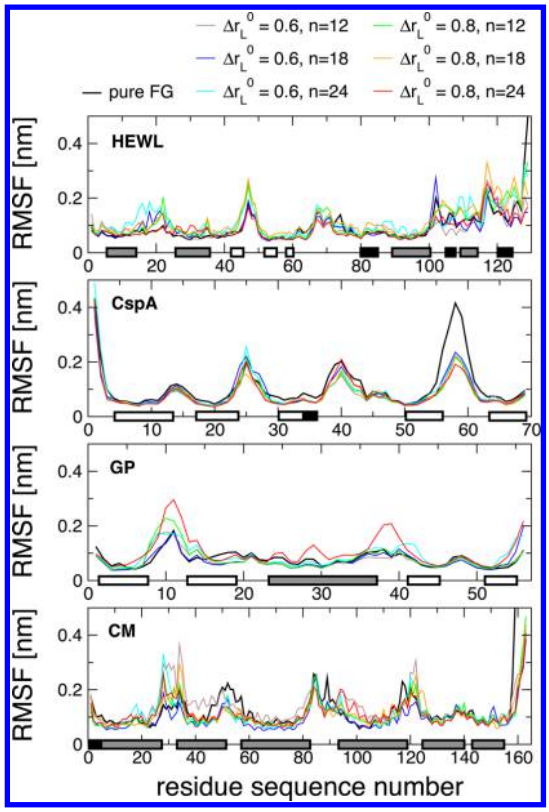

Figure 10. Atom-positional root-mean-square fluctuations (RMSF) of the backbone C_α atoms of the HEWL, CspA, GP, and CM proteins in pure FG solvent or in FG/CG mixtures using FBMS restraints. The bars on the abscissa indicate the secondary structure elements, i.e., 3_{10}-helix (black), α-helix (gray), and β-strands (white). The color coding is as in Figure 9. See Table 6 for the parameters corresponding to the different simulations.

unstructured part of the protein between the first two helices. At the C-terminus, the differences reach up to 0.4 nm for both backbone and side chains.

The secondary structure evolution of the four proteins during the different simulations is shown in Figures S8–S11. The secondary structures of the proteins in the FG/CG simulations are also found to agree well with the results from the purely FG simulations. The total numbers of observed intraprotein hydrogen bonds and the total occurrences of these bonds during the protein simulations are shown in Figure 12, considering separately backbone–backbone (bb–bb), backbone–side chain (bb–sc), and side chain–side chain (sc–sc) hydrogen bonds. The results from the FG/CG simulations with FBMS restraints are again compared to the purely FG simulations as well as to FG/CG solvent simulations with an FG solvation layer of 0.8 nm restrained to the COM of the solute.[60] No significant differences occur between the simulations when considering the total numbers of bb–bb hydrogen bonds. The bb–sc and sc–sc hydrogen bonds show, in general, slightly more variations. In particular, the simulations with COM restraints tend to yield higher occurrences of bb–sc hydrogen bonds for HEWL and CM and of sc–sc hydrogen bonds for CM, compared to the FBMS simulations. These differences are small and non-systematic across the four proteins.

The local volumetric fractions of FG solvent molecules and CG solvent beads around the surface of the proteins are shown in Figure S12. They do not present major differences between the different simulations. On the other hand, the corresponding curves for the splitting entropy measure $M(R^{SW})$ displayed in Figure 13, exhibit significant differences at distances larger than 1.0 nm from the surface of the proteins when comparing simulations with different exponents n. At short distance from the surface of the protein, the $M(R^{SW})$ curves for n = 18 and 24 converge to similar values close to 1, with slightly lower values for n = 12. The results considering different initial layer thicknesses Δr_L^0 are very similar.

The restraining energies V^{att} per FG water molecule, reported in Table 6, are an order of magnitude lower than the thermal energy k_BT (2.5 kJ mol^{-1} at 298 K). For the CG solvent beads, the restraining energies V^{rep} are 2 to 3 orders of magnitude lower than k_BT. However, the distributions of the restraining energies of the FG solvent molecules, displayed in Figure S13, reveal that some FG molecules are affected by attractive restraints with energies up to 60 kJ mol^{-1}, whereas some CG beads are affected by repulsive restraints with energies up to 10 kJ mol^{-1}. The CG solvent beads interact, on average, an order of magnitude more weakly with the protein than in corresponding purely CG solvent simulations, in which the average values of $V_{nonb}^{su\text{-}CG}$ per CG bead for HEWL, CspA, GP, and CM were −1.6, −2.3, −2.3, and −2.2 kJ mol^{-1}, respectively (values calculated based on the trajectories of ref 66). The intraprotein potential energy from the fully

DOI: 10.1021/acs.jctc.5b00406
J. Chem. Theory Comput. 2015, 11, 5447–5463

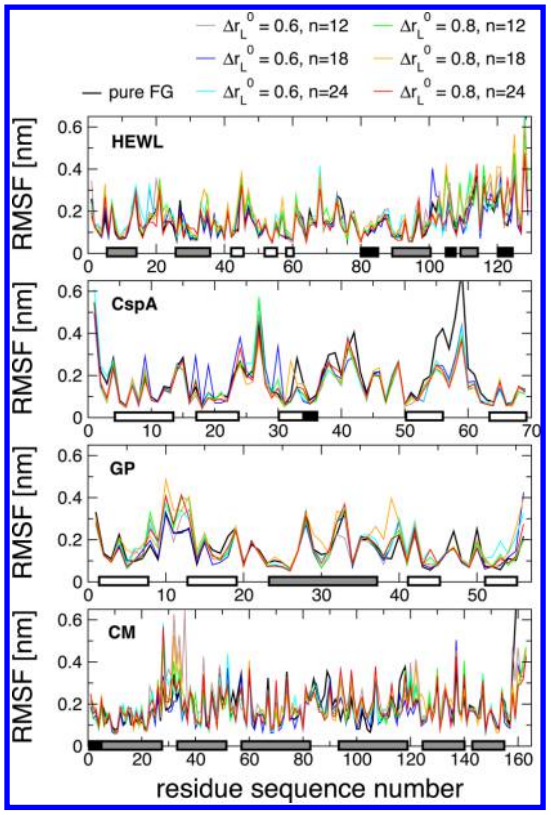

Figure 11. Atom-positional root-mean-square fluctuations (RMSF) of the last atom of each side chain of the HEWL, CspA, GP, and CM proteins in pure FG solvent or in FG/CG mixtures using FBMS restraints. The bars on the abscissa indicate the secondary structure elements, i.e., 3_{10}-helix (black), α-helix (gray), and β-strands (white). The color coding is as in Figure 9. See Table 6 for the parameters corresponding to the different simulations.

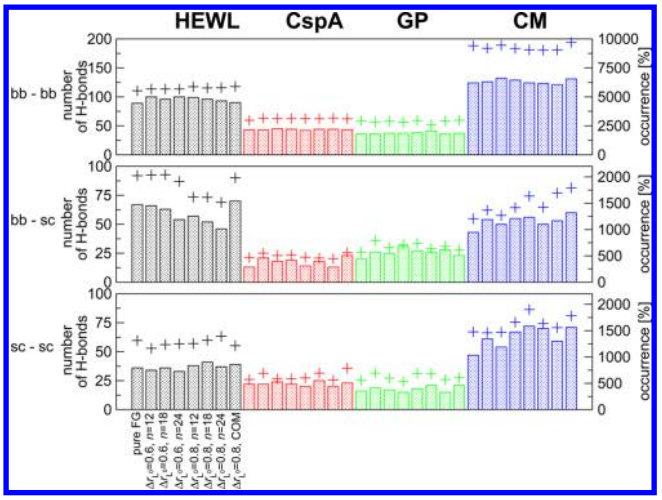

Figure 12. Total numbers (bars, left scale) and total occurrences (crosses, right scale) of hydrogen bonds in the simulations of proteins HEWL, CspA, GP, and CM, averaged separately for backbone−backbone (bb−bb), backbone−side chain (bb−sc), and side chain−side chain (sc−sc) hydrogen bonds. For each protein, the simulations are ordered from left to right: system with pure FG solvent, FG/CG system with FBMS restraints involving an FG water layer of initial thickness Δr_L^0 = 0.6 nm and an exponent n = 12, system with Δr_L^0 = 0.6 nm and n = 18, system with Δr_L^0 = 0.6 nm and n = 24, system with Δr_L^0 = 0.8 nm and n = 12, system with Δr_L^0 = 0.8 nm and n = 18, system with Δr_L^0 = 0.8 nm and n = 24, and system with Δr_L^0 = 0.8 nm using restraints to the COM of the protein.[60] See Table 6 for the parameters corresponding to the different FBMS simulations.

atomistic simulations, shown in Figure S14, is also reproduced in the FBMS simulations.

4. CONCLUSIONS

In this article, we introduced an algorithm termed flexible boundaries for multiresolution solvation (FBMS), for performing MD simulations of an atomistic biomolecular solute in a multiresolution FG/CG solvent mixture. It involves: (i) a three-region layering of the solvent around the solute involving an FG layer, surrounded by a mixed FG−CG buffer layer, itself surrounded by a bulk CG region; (ii) a definition of the layer boundaries that relies on an effective distance to the solute surface. The layering is enforced by means of half-harmonic distance restraints, attractive for the FG molecules and repulsive for the CG beads. The surface-weighted distance is defined by inverse-nth power averaging over the distances to all non-hydrogen solute atoms. For a sufficiently high exponent n, this metric approximates well the distance to the closest solute atom, leading to a layering that follows closely the features of the solute surface and their changes in time, and leads to a spreading of the restraint forces over multiple surface atoms. A restraint-free region at intermediate surface-weighted distances enables the formation of the buffer layer, where the two types of solvents can mix freely.

Because the layering is defined in terms of an approximate distance to the solute surface while the buffer region can absorb or release FG molecules into or out of the FG layer, this layer is flexible and adapted to the shape of the solute, and remains so irrespective of possible solute conformational changes. Applying solely attractive or solely repulsive restraints is not sufficient to guarantee the separation of the two types of solvents, i.e., the absence of CG beads in the FG layer and of FG molecules in the CG bulk region. The explicit separation of the FG and CG solvents using restraints in the FBMS method offers two specific advantages: (i) the FG molecules and CG beads are not required to demix spontaneously, so the algorithm is applicable to models presenting physically realistic mixing properties;[70,74] (ii) the CG beads are excluded from the solvation layer and the FG molecules from the bulk region, so there is no need for the calibration and application of an extra thermodynamic force[75,76] to regulate the corresponding distributions.

The algorithm was tested and validated using the GROMOS 54A7 force field[84] and the associated FG (SPC model[73]) and CG (polarizable CGW model[78]) water models. Based on the results, a recommended combination of parameters is proposed for the practical application of the restraints in biomolecular simulations.

The exponent n should be at least 12 to ensure a sufficiently close similarity between the surface-weighted distance and the exact surface distance over the relevant range. Values of 12 or 18, possibly 24, seem to be equally acceptable, but higher values may limit the spread of the restraint forces over solute surface atoms and possibly lead to numerical instabilities in the surface-weighted distance calculation at finite precision.

For the employed SPC and CGW models, which evidence physically realistic mixing properties,[74] relatively high restraining force constants on the order of 50−500 kJ mol^{-1} nm^{-2} for K^{att} and 500−1000 kJ mol^{-1} nm^{-2} for K^{rep} are required to keep the two solvent types well separated. In the present work, the combination (K^{att}, K^{rep}) = (300, 600) kJ mol^{-1} nm^{-2} gave good results.

DOI: 10.1021/acs.jctc.5b00406
J. Chem. Theory Comput. 2015, 11, 5447−5463

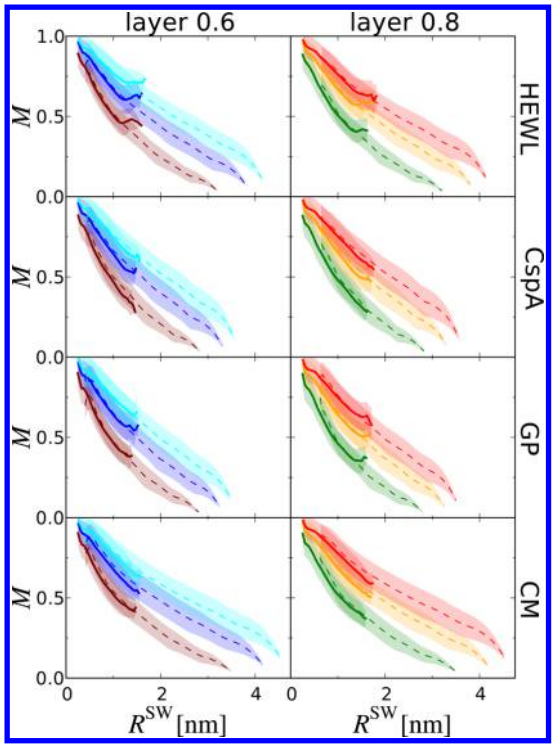

Figure 13. Splitting entropy measures M for the HEWL, CspA, GP, and CM proteins in FG/CG water mixtures with FBMS restraints. The results are calculated using eq 10 based on 20 ns simulations for two different initial thicknesses Δr_L^0 of the FG layer (left and right columns, value in nanometers). The splitting entropy measure is averaged over all FG molecules (solid red lines) or over all CG beads (dashed black lines) and displayed as $M(R^{SW})$, where R^{SW} corresponds to the surface-weighted distance between solute and solvent, and the bin width was set to 0.06 nm. The shaded areas around the curves indicate the standard deviations around the mean. In all cases, (K^{att}, K^{rep}) = (300, 600) kJ mol^{-1} nm^{-2}, $R^{att} = \Delta r_L^0 + 0.2$ nm, and $R^{rep} = \Delta r_L^0 + 0.1$ nm. The color coding is as in Figure 9.

The initial FG layer thickness Δr_L^0 and the buffer thickness $\Delta r_B = R^{att} - R^{rep}$ must be chosen such that for all accessible solute conformations, e.g., α-helical and extended conformations of a peptide, the FG layer never becomes depleted of FG molecules, and the buffer layer of either FG molecules or CG beads. When using an exponent $n \geq 12$, the results suggest that the choices $R^{att} = \Delta r_L^0 + 0.2$ nm and $R^{rep} = \Delta r_L^0 + 0.1$ nm are appropriate. The initial layer thickness Δr_L^0 itself should be set based on the size of the FG molecules. For example, the values of 0.6 or 0.8 nm employed for the aqueous biomolecules in the present study correspond to including about 2 to 3 solvation shells of FG molecules around the solute, and are sufficient to preserve the properties of the biomolecules as compared to purely FG simulations.

The proposed method is expected to deliver a speed-up compared to the simulations involving a fully FG solvation because of the largely reduced number of solute−solvent and solvent−solvent interactions when using a supra-molecular CG solvent. On the other hand, the calculation of the restraining forces requires the calculation of all distances between non-hydrogen solute atoms and solvent molecules or beads. In the present simple, nonparallelized implementation of the algorithm, a speed-up of 1.8−7.2 is reached.

A validation was performed using FBMS simulations of four proteins in multiresolution FG/CG mixtures that relied on the recommended parameter settings. The structural, energetic, and solvation properties of the proteins in these simulations, including atom-positional RMSD and RMSF values, radius of gyration, interaction potential energies, and hydrogen-bonding characteristics, were found to be very similar to those observed in corresponding fully FG simulations.

■ ASSOCIATED CONTENT

Supporting Information

The Supporting Information is available free of charge on the ACS Publications website at DOI: 10.1021/acs.jctc.5b00406.

Additional results for the FG/CG pure-water systems (Figures S1 and S2); comparison between restraining to the solute center of mass and to the solute surface in a simulation of the G-protein (Figure S3); additional simulated properties for the deca-alanine peptide (Figures S4 and S5); additional simulated properties for the four proteins (Figures S6−S14) (PDF).

■ AUTHOR INFORMATION

Corresponding Author

*E-mail: wfvgn@ethz.ch.

Present Address

†(O.M.S.) Department of Electrical Engineering and Information Technology, Swiss Federal Institute of Technology ETH, 8006 Zürich, Switzerland.

Funding

This work was financially supported by the National Center of Competence in Research (NCCR) in structural biology, the Swiss National Science Foundation (grant no. 200020-137827), and the European Research Council (grant no. 228076).

Notes

The authors declare no competing financial interest.

■ ACKNOWLEDGMENTS

The authors would like to thank Andreas Eichenberger and Sereina Riniker for providing the molecular dynamics trajectories corresponding to the biomolecules solvated in pure FG and pure CG water.

■ REFERENCES

(1) Müller-Plathe, F. *ChemPhysChem* **2002**, *3*, 754−769.
(2) Nielsen, S. O.; Lopez, C. F.; Srinivas, G.; Klein, M. L. *J. Phys.: Condens. Matter* **2004**, *16*, R481−R512.
(3) Marrink, S. J.; Risselada, H. J.; Yefimov, S.; Tieleman, D. P.; de Vries, A. H. *J. Phys. Chem. B* **2007**, *111*, 7812−7824.
(4) Voth, G. A. *Coarse-Graining of Condensed Phase and Biomolecular Systems*; CRC Press: Boca Raton, FL, 2008.
(5) Riniker, S.; Allison, J. R.; van Gunsteren, W. F. *Phys. Chem. Chem. Phys.* **2012**, *14*, 12423−12430.
(6) Shen, H.; Xia, Z.; Li, G.; Ren, P. *Annu. Rep. Comput. Chem.* **2012**, *8*, 129−148.
(7) Noid, W. G. *J. Chem. Phys.* **2013**, *139*, 090901.
(8) Ingolfsson, H. I.; Lopez, C. A.; Uusitalo, J. J.; de Jong, D. H.; Gopal, S. M.; Periole, X.; Marrink, S. J. *WIREs Comput. Mol. Sci.* **2014**, *4*, 225−248.
(9) van Gunsteren, W. F.; Berendsen, H. J. C. *Mol. Phys.* **1977**, *34*, 1311−1327.
(10) van Gunsteren, W. F.; Berendsen, H. J. C.; Rullmann, J. A. C. *Mol. Phys.* **1981**, *44*, 69−95.
(11) Meier, K.; Choutko, A.; Dolenc, J.; Eichenberger, A. P.; Riniker, S.; van Gunsteren, W. F. *Angew. Chem., Int. Ed.* **2013**, *52*, 2820−2834.

DOI: 10.1021/acs.jctc.5b00406
J. Chem. Theory Comput. 2015, 11, 5447−5463

(12) van Gunsteren, W. F.; Berendsen, H. J. C. *Mol. Phys.* **1982**, *45*, 637−647.
(13) Louis, A. A. *J. Phys.: Condens. Matter* **2002**, *14*, 9187−9206.
(14) Johnson, M. E.; Head-Gordon, T.; Louis, A. A. *J. Chem. Phys.* **2007**, *126*, 144509.
(15) Levitt, M.; Lifson, S. *J. Mol. Biol.* **1969**, *46*, 269−279.
(16) Hadley, K. R.; McCabe, C. *J. Phys. Chem. B* **2010**, *114*, 4590−4599.
(17) Larini, L.; Lu, L.; Voth, G. A. *J. Chem. Phys.* **2010**, *132*, 164107.
(18) Wu, Z.; Cui, Q.; Yethiraj, A. *J. Phys. Chem. B* **2010**, *114*, 10524−10529.
(19) Darré, L.; Machado, M. R.; Dans, P. D.; Herrera, F. E.; Pantano, S. *J. Chem. Theory Comput.* **2010**, *6*, 3793−3807.
(20) Yesylevskyy, S. O.; Schäfer, L. V.; Sengupta, D.; Marrink, S.-J *PLoS Comput. Biol.* **2010**, *6*, e1000810.
(21) Fogarty, J. C.; Chiu, S.-W.; Kirby, P.; Jakobsson, E.; Pandit, S. A. *J. Phys. Chem. B* **2014**, *118*, 1603−1611.
(22) Chiu, S.-W.; Scott, H. L.; Jakobsson, E. *J. Chem. Theory Comput.* **2010**, *6*, 851−863.
(23) Orsi, M. *Mol. Phys.* **2014**, *112*, 1566−1576.
(24) Peter, A. K.; Pivkin, V. *J. Chem. Phys.* **2014**, *141*, 164506.
(25) Jacobson, L. C.; Kirby, R. M.; Molinero, V. *J. Phys. Chem. B* **2014**, *118*, 8190−8202.
(26) Allison, J. R.; Riniker, S.; van Gunsteren, W. F. *J. Chem. Phys.* **2012**, *136*, 054505.
(27) Szklarczyk, O. M.; Arvaniti, E.; van Gunsteren, W. F. *J. Comput. Chem.* **2015**, *36*, 1311−1321.
(28) Baschnagel, J.; Binder, K.; Doruker, P.; Gusev, A. A.; Hahn, O.; Kremer, K.; Mattice, W. L.; Müller-Plathe, F.; Murat, M.; Paul, W.; Santos, S.; Suter, U. W.; Tries, V. *Viscoelasticity, Atomistic Models, Statistical Chemistry*; Springer: Berlin, 2000; pp 41−156.
(29) Marrink, S. J.; de Vries, A. H.; Mark, A. E. *J. Phys. Chem. B* **2004**, *108*, 750−760.
(30) Orsi, M.; Haubertin, D. Y.; Sanderson, W. E.; Essex, J. W. *J. Phys. Chem. B* **2008**, *112*, 802−815.
(31) Han, W.; Wan, C. K.; Wu, Y. D. *J. Chem. Theory Comput.* **2008**, *4*, 1891−1901.
(32) Huertas, M. L.; Navarro, S.; Lopez Martinez, M. C.; García de la Torre, J. *Biophys. J.* **1997**, *73*, 3142−3153.
(33) Morriss-Andrews, A.; Rottler, J.; Plotkin, S. S. *J. Chem. Phys.* **2010**, *132*, 035105.
(34) Ouldridge, T. E.; Louis, A. A.; Doye, J. P. K. *J. Chem. Phys.* **2011**, *134*, 085101.
(35) Takada, S. *Curr. Opin. Struct. Biol.* **2012**, *22*, 130−137.
(36) Han, W.; Wu, Y.-D. *J. Chem. Theory Comput.* **2007**, *3*, 2146−2161.
(37) Villa, A.; Peter, C.; van der Vegt, N. F. A. *J. Chem. Theory Comput.* **2010**, *6*, 2434−2444.
(38) Wu, Z.; Cui, Q.; Yethiraj, A. *J. Chem. Theory Comput.* **2011**, *7*, 3793−3802.
(39) Hadley, K. R.; McCabe, C. *Mol. Simul.* **2012**, *38*, 671−681.
(40) Lazaridis, T.; Versace, R. *Isr. J. Chem.* **2014**, *54*, 1074−1083.
(41) Warshel, A.; Levitt, M. *J. Mol. Biol.* **1976**, *103*, 227−249.
(42) Field, M. J.; Bash, P. A.; Karplus, M. *J. Comput. Chem.* **1990**, *11*, 700−733.
(43) Tschöp, W.; Kremer, K.; Hahn, O.; Batoulis, J.; Bürger, T. *Acta Polym.* **1998**, *49*, 75−79.
(44) Milano, G.; Müller-Plathe, F. *J. Phys. Chem. B* **2005**, *109*, 18609−18619.
(45) Izvekov, S.; Voth, G. A. *J. Phys. Chem. B* **2005**, *109*, 2469−2473.
(46) Hess, B.; Salvador, L.; van der Vegt, N.; Kremer, K. *Soft Matter* **2006**, *2*, 409−414.
(47) Heath, A. P.; Kavraki, L. E.; Clementi, C. *Proteins: Struct., Funct., Genet.* **2007**, *68*, 646−661.
(48) Rzepiela, A. J.; Schafter, L. V.; Goga, N.; Risselada, H. J.; De Vries, A. H.; Marrink, S J. *J. Comput. Chem.* **2010**, *31*, 1333−1343.
(49) Samiotakis, A.; Homouz, D.; Cheung, M. S. *J. Chem. Phys.* **2010**, *132*, 175101.
(50) Christen, M.; van Gunsteren, W. F. *J. Chem. Phys.* **2006**, *124*, 154106.
(51) Lyman, E.; Ytreberg, F. M.; Zuckerman, D. M. *Phys. Rev. Lett.* **2006**, *96*, 028105.
(52) Lyman, E.; Zuckerman, D. M. *J. Chem. Theory Comput.* **2006**, *2*, 656−666.
(53) Praprotnik, M.; Delle Site, L.; Kremer, K. *J. Chem. Phys.* **2005**, *123*, 224106.
(54) Ensing, B.; Nielsen, S. O.; Moore, P. B.; Klein, M. L.; Parrinello, M. *J. Chem. Theory Comput.* **2007**, *3*, 1100−1105.
(55) Praprotnik, M.; Site, L. D.; Kremer, K. *Annu. Rev. Phys. Chem.* **2008**, *59*, 545−571.
(56) Wagoner, J. A.; Pande, V. S. *J. Chem. Phys.* **2011**, *134*, 214103.
(57) Wagoner, J. A.; Pande, V. S. *J. Chem. Phys.* **2013**, *139*, 234114.
(58) Zavadlav, J.; Melo, M. N.; Cunha, A. V.; de Vries, A. H.; Marrink, S. J.; Praprotnik, M. *J. Chem. Theory Comput.* **2014**, *10*, 2591−2598.
(59) Zavadlav, J.; Melo, M. N.; Marrink, S. J.; Praprotnik, M. *J. Chem. Phys.* **2014**, *140*, 054114.
(60) Riniker, S.; Eichenberger, A. P.; van Gunsteren, W. F. *J. Phys. Chem. B* **2012**, *116*, 8873−8879.
(61) Rzepiela, A. J.; Louhivuori, M.; Peter, C.; Marrink, S. *Phys. Chem. Chem. Phys.* **2011**, *13*, 10437−10448.
(62) Sokkar, P.; Choi, S. M.; Rhee, Y. M. *J. Chem. Theory Comput.* **2013**, *9*, 3728−3739.
(63) Gonzalez, H. C.; Darré, L.; Pantano, S. *J. Phys. Chem. B* **2013**, *117*, 14438−14448.
(64) Izvekov, S.; Voth, G. A. *J. Phys. Chem. B* **2005**, *109*, 2469−2473.
(65) Wu, Z.; Cui, Q.; Yethiraj, A. *J. Phys. Chem. Lett.* **2011**, *2*, 1794−1798.
(66) Riniker, S.; Eichenberger, A. P.; van Gunsteren, W. F. *Eur. Biophys. J.* **2012**, *41*, 647−661.
(67) Wassenaar, T. A.; Ingolfsson, H. I.; Priess, M.; Marrink, S. J.; Schäfer, L. V. *J. Phys. Chem. B* **2013**, *117*, 3516−3530.
(68) Huang, W.; Riniker, S.; van Gunsteren, W. F. *J. Chem. Theory Comput.* **2014**, *10*, 2213−2223.
(69) Huang, W.; Hansen, N.; van Gunsteren, W. F. *Helv. Chim. Acta* **2013**, *97*, 1591−1605.
(70) Orsi, M.; Ding, W.; Palaiokostas, M. *J. Chem. Theory Comput.* **2014**, *10*, 4684−4693.
(71) Han, W.; Schulten, K. *J. Chem. Theory Comput.* **2012**, *8*, 4413−4424.
(72) Lin, Z.; Riniker, S.; van Gunsteren, W. F. *J. Chem. Theory Comput.* **2013**, *9*, 1328−1333.
(73) Berendsen, H. J. C.; Postma, J. P. M.; van Gunsteren, W. F.; Hermans, J. Interaction models for water in relation to protein hydration. *Intermolecular Forces* **1981**, *14*, 331−342.
(74) Riniker, S.; van Gunsteren, W. F. *J. Chem. Phys.* **2012**, *137*, 044120.
(75) Praprotnik, M.; Poblete, S.; Kremer, K. *J. Stat. Phys.* **2011**, *145*, 946−966.
(76) Fritsch, S.; Poblete, S.; Junghans, C.; Ciccotti, G.; Delle Site, L.; Kremer, K. *Phys. Rev. Lett.* **2012**, *108*, 170602.
(77) Potestio, R.; Fritsch, S.; Espanol, P.; Delgado-Buscalioni, R.; Kremer, K.; Everaers, R.; Donadio, D. *Phys. Rev. Lett.* **2013**, *110*, 108301.
(78) Riniker, S.; van Gunsteren, W. F. *J. Chem. Phys.* **2011**, *134*, 084110.
(79) Nilges, M. *Proteins: Struct., Funct., Genet.* **1993**, *17*, 297−309.
(80) Nilges, M.; Macias, M. J.; O'Donoghue, S. I.; Oschkinat, H. *J. Mol. Biol.* **1997**, *269*, 408−422.
(81) Dominguez, C.; Boelens, R.; Bonvin, A. M. J. J. *J. Am. Chem. Soc.* **2003**, *125*, 1731−1737.
(82) De Vries, S. J.; van Dijk, M.; Bonvin, A. M. J. J. *Nat. Protoc.* **2010**, *5*, 883−897.
(83) Horn, R. A.; Johnson, C. R. *Matrix Analysis*; Cambridge University Press: New York, 2013; Chapter 5, pp 313−386.
(84) Schmid, N.; Eichenberger, A. P.; Choutko, A.; Riniker, S.; Winger, M.; Mark, A. E.; van Gunsteren, W. F. *Eur. Biophys. J.* **2011**, *40*, 843−856.
(85) Eichenberger, A. P.; Allison, J. R.; Dolenc, J.; Geerke, D. P.; Horta, B. A. C.; Meier, K.; Oostenbrink, C.; Schmid, N.; Steiner, D.; Wang, D.; van Gunsteren, W. F. *J. Chem. Theory Comput.* **2011**, *7*, 3379−3390.

DOI: 10.1021/acs.jctc.5b00406
J. Chem. Theory Comput. 2015, 11, 5447−5463

(86) Hansen, H.; Daura, X.; Hünenberger, P. H. *J. Chem. Theory Comput.* **2010**, *6*, 2598−2621.
(87) Artymiuk, P. J.; Blake, C. C. F.; Rice, D. W.; Wilson, K. S. *Acta Crystallogr., Sect. B: Struct. Crystallogr. Cryst. Chem.* **1982**, *38*, 778−783.
(88) Schindelin, H.; Jiang, W.; Inouye, M.; Heinemann, U. *Proc. Natl. Acad. Sci. U. S. A.* **1994**, *91*, 5119−5123.
(89) Gallagher, T.; Alexander, P.; Bryan, P.; Gilliland, G. L. *Biochemistry* **1994**, *33*, 4721−4729.
(90) Okvist, M.; Dey, R.; Sasso, S.; Grahn, E.; Kast, P.; Krengel, U. *J. Mol. Biol.* **2006**, *357*, 1483−1499.
(91) *GROMOS*; BIOMOS: Zürich, Switzerland. http://www.gromos.net.
(92) Schmid, N.; Christ, C. D.; Christen, M.; Eichenberger, A. P.; van Gunsteren, W. F. *Comput. Phys. Commun.* **2011**, *183*, 890−903.
(93) Ryckaert, J. P.; Ciccotti, G.; Berendsen, H. J. C. *J. Comput. Phys.* **1977**, *23*, 327−341.
(94) Hockney, R. W. *Methods Comput. Phys.* **1970**, *9*, 136−211.
(95) Berendsen, H. J. C.; Postma, J. P. M.; van Gunsteren, W. F.; DiNola, A.; Haak, J. R. *J. Chem. Phys.* **1984**, *81*, 3684−3690.
(96) van Gunsteren, W. F.; Billeter, S. R.; Eising, A. A.; Hünenberger, P. H.; Krüger, P. K. H. C.; Mark, A. E.; Scott, W. R. P.; Tironi, I. G. *Biomolecular Simulation: The GROMOS96 Manual and User Guide*; Vdf Hochschulverlag AG an der ETH Zürich: Zürich, Switzerland, 1996; p II(133).
(97) Christen, M.; Kunz, A. P. E.; van Gunsteren, W. F. *J. Phys. Chem. B* **2006**, *110*, 8488−8498.
(98) Berendsen, H. J. C.; van Gunsteren, W. F.; Zwinderman, H. R. J.; Geurtsen, R. G.; Ann, N. Y. *Ann. N. Y. Acad. Sci.* **1986**, *482*, 269−286.
(99) Onsager, L. *J. Am. Chem. Soc.* **1936**, *58*, 1486−1493.
(100) Barker, J. A.; Watts, R. O. *Mol. Phys.* **1973**, *26*, 789−792.
(101) van der Spoel, D.; van Maaren, P.; Berendsen, H. J. C. *J. Chem. Phys.* **1998**, *108*, 10220.
(102) Lide, D. R. *CRC Handbook of Chemistry and Physics*; CRC Press: Boca Raton, FL, 2012; p 6(14).

DOI: 10.1021/acs.jctc.5b00406
J. Chem. Theory Comput. 2015, 11, 5447−5463